# Determination of $|V\_ub|$ from the Measurement of the Inclusive Charmless Semileptonic Branching Ratio of b hadrons

R. Barate, D. Buskulic, D. Decamp, P. Ghez, C. Goy, J P. Lees, A. Lucotte, F. Martin, E. Merle, M N. Minard, et al.

LABORATOIRE EUROPEEN POUR LA PHYSIQUE DES PARTICULES (CERN)

CERN-EP/98-067
May 5, 1998

# Determination of $|V_{ub}|$ from the Measurement of the Inclusive Charmless Semileptonic Branching Ratio of b hadrons

The ALEPH Collaboration [1]

**Abstract**

From a study of the kinematic properties of the final state produced in the semileptonic decays $b \to X\ell\nu_\ell$, the inclusive charmless semileptonic branching ratio of b hadrons is measured. With a sample of 3.6 million hadronic Z decays recorded between 1992 and 1995 with the ALEPH detector at LEP, the value $Br(b \to X_u\ell\nu_\ell)$ is determined to be $(1.73 \pm 0.55_{stat} \pm 0.55_{syst}) \times 10^{-3}$, where $X_u$ represents any charmless hadronic state and b is a mixture of b hadrons weighted by their production rates. This measurement yields the result

$$|V_{ub}|^2 = (18.68 \pm 5.94_{stat} \pm 5.94_{syst} \pm 1.45_{HQE}) \times 10^{-6},$$

where the last error comes from the conversion of the branching ratio to the CKM matrix element squared.

*(Submitted to The European Physical Journal C)*

[1] See next pages for the list of authors

# The ALEPH Collaboration

R. Barate, D. Buskulic, D. Decamp, P. Ghez, C. Goy, J.-P. Lees, A. Lucotte, E. Merle, M.-N. Minard, J.-Y. Nief, B. Pietrzyk

*Laboratoire de Physique des Particules (LAPP), IN$^2$P$^3$-CNRS, F-74019 Annecy-le-Vieux Cedex, France*

R. Alemany, G. Boix, M.P. Casado, M. Chmeissani, J.M. Crespo, M. Delfino, E. Fernandez, M. Fernandez-Bosman, Ll. Garrido,[15] E. Graugès, A. Juste, M. Martinez, G. Merino, R. Miquel, Ll.M. Mir, I.C. Park, A. Pascual, I. Riu, F. Sanchez

*Institut de Física d'Altes Energies, Universitat Autònoma de Barcelona, E-08193 Bellaterra (Barcelona), Spain*[7]

A. Colaleo, D. Creanza, M. de Palma, G. Gelao, G. Iaselli, G. Maggi, M. Maggi, S. Nuzzo, A. Ranieri, G. Raso, F. Ruggieri, G. Selvaggi, L. Silvestris, P. Tempesta, A. Tricomi,[3] G. Zito

*Dipartimento di Fisica, INFN Sezione di Bari, I-70126 Bari, Italy*

X. Huang, J. Lin, Q. Ouyang, T. Wang, Y. Xie, R. Xu, S. Xue, J. Zhang, L. Zhang, W. Zhao

*Institute of High-Energy Physics, Academia Sinica, Beijing, The People's Republic of China*[8]

D. Abbaneo, U. Becker, P. Bright-Thomas, D. Casper, M. Cattaneo, V. Ciulli, G. Dissertori, H. Drevermann, R.W. Forty, M. Frank, R. Hagelberg, J.B. Hansen, J. Harvey, P. Janot, B. Jost, I. Lehraus, P. Mato, A. Minten, L. Moneta,[21] A. Pacheco, F. Ranjard, L. Rolandi, D. Rousseau, D. Schlatter, M. Schmitt,[20] O. Schneider, W. Tejessy, F. Teubert, I.R. Tomalin, H. Wachsmuth

*European Laboratory for Particle Physics (CERN), CH-1211 Geneva 23, Switzerland*

Z. Ajaltouni, F. Badaud, G. Chazelle, O. Deschamps, A. Falvard, C. Ferdi, P. Gay, C. Guicheney, P. Henrard, J. Jousset, B. Michel, S. Monteil, J-C. Montret, D. Pallin, P. Perret, F. Podlyski, J. Proriol, P. Rosnet

*Laboratoire de Physique Corpusculaire, Université Blaise Pascal, IN$^2$P$^3$-CNRS, Clermont-Ferrand, F-63177 Aubière, France*

J.D. Hansen, J.R. Hansen, P.H. Hansen, B.S. Nilsson, B. Rensch, A. Wäänänen

*Niels Bohr Institute, DK-2100 Copenhagen, Denmark*[9]

G. Daskalakis, A. Kyriakis, C. Markou, E. Simopoulou, I. Siotis, A. Vayaki

*Nuclear Research Center Demokritos (NRCD), GR-15310 Attiki, Greece*

A. Blondel, G. Bonneaud, J.-C. Brient, P. Bourdon, A. Rougé, M. Rumpf, A. Valassi,[6] M. Verderi, H. Videau

*Laboratoire de Physique Nucléaire et des Hautes Energies, Ecole Polytechnique, IN$^2$P$^3$-CNRS, F-91128 Palaiseau Cedex, France*

E. Focardi, G. Parrini, K. Zachariadou

*Dipartimento di Fisica, Università di Firenze, INFN Sezione di Firenze, I-50125 Firenze, Italy*

M. Corden, C. Georgiopoulos, D.E. Jaffe

*Supercomputer Computations Research Institute, Florida State University, Tallahassee, FL 32306-4052, USA* [13,14]

A. Antonelli, G. Bencivenni, G. Bologna,[4] F. Bossi, P. Campana, G. Capon, F. Cerutti, V. Chiarella, G. Felici, P. Laurelli, G. Mannocchi,[5] F. Murtas, G.P. Murtas, L. Passalacqua, M. Pepe-Altarelli

*Laboratori Nazionali dell'INFN (LNF-INFN), I-00044 Frascati, Italy*

L. Curtis, A.W. Halley, J.G. Lynch, P. Negus, V. O'Shea, C. Raine, J.M. Scarr, K. Smith, P. Teixeira-Dias, A.S. Thompson, E. Thomson

*Department of Physics and Astronomy, University of Glasgow, Glasgow G12 8QQ, United Kingdom*[10]

O. Buchmüller, S. Dhamotharan, C. Geweniger, G. Graefe, P. Hanke, G. Hansper, V. Hepp, E.E. Kluge, A. Putzer, J. Sommer, K. Tittel, S. Werner, M. Wunsch

*Institut für Hochenergiephysik, Universität Heidelberg, D-69120 Heidelberg, Germany*[16]

R. Beuselinck, D.M. Binnie, W. Cameron, P.J. Dornan,[2] M. Girone, S. Goodsir, E.B. Martin, N. Marinelli, A. Moutoussi, J. Nash, J.K. Sedgbeer, P. Spagnolo, M.D. Williams

*Department of Physics, Imperial College, London SW7 2BZ, United Kingdom*[10]

V.M. Ghete, P. Girtler, E. Kneringer, D. Kuhn, G. Rudolph

*Institut für Experimentalphysik, Universität Innsbruck, A-6020 Innsbruck, Austria*[18]

C.K. Bowdery, P.G. Buck, P. Colrain, G. Crawford, A.J. Finch, F. Foster, G. Hughes, R.W.L. Jones, N.A. Robertson, M.I. Williams

*Department of Physics, University of Lancaster, Lancaster LA1 4YB, United Kingdom*[10]

I. Giehl, C. Hoffmann, K. Jakobs, K. Kleinknecht, G. Quast, B. Renk, E. Rohne, H.-G. Sander, P. van Gemmeren, C. Zeitnitz

*Institut für Physik, Universität Mainz, D-55099 Mainz, Germany*[16]

J.J. Aubert, C. Benchouk, A. Bonissent, G. Bujosa, J. Carr,[2] P. Coyle, F. Etienne, O. Leroy, F. Motsch, P. Payre, M. Talby, A. Sadouki, M. Thulasidas, K. Trabelsi

*Centre de Physique des Particules, Faculté des Sciences de Luminy, IN$^2$P$^3$-CNRS, F-13288 Marseille, France*

M. Aleppo, M. Antonelli, F. Ragusa

*Dipartimento di Fisica, Università di Milano e INFN Sezione di Milano, I-20133 Milano, Italy*

R. Berlich, W. Blum, V. Büscher, H. Dietl, G. Ganis, H. Kroha, G. Lütjens, C. Mannert, W. Männer, H.-G. Moser, S. Schael, R. Settles, H. Seywerd, H. Stenzel, W. Wiedenmann, G. Wolf

*Max-Planck-Institut für Physik, Werner-Heisenberg-Institut, D-80805 München, Germany*[16]

J. Boucrot, O. Callot, S. Chen, A. Cordier, M. Davier, L. Duflot, J.-F. Grivaz, Ph. Heusse, A. Höcker, A. Jacholkowska, D.W. Kim,[12] F. Le Diberder, J. Lefrançois, A.-M. Lutz, M.-H. Schune, E. Tournefier, J.-J. Veillet, I. Videau, D. Zerwas

*Laboratoire de l'Accélérateur Linéaire, Université de Paris-Sud, IN$^2$P$^3$-CNRS, F-91898 Orsay Cedex, France*

P. Azzurri, G. Bagliesi,[2] G. Batignani, S. Bettarini, T. Boccali, C. Bozzi, G. Calderini, M. Carpinelli, M.A. Ciocci, R. Dell'Orso, R. Fantechi, I. Ferrante, L. Foà,[1] F. Forti, A. Giassi, M.A. Giorgi, A. Gregorio, F. Ligabue, A. Lusiani, P.S. Marrocchesi, A. Messineo, F. Palla, G. Rizzo, G. Sanguinetti, A. Sciabà, G. Sguazzoni, R. Tenchini, G. Tonelli,[19] C. Vannini, A. Venturi, P.G. Verdini

*Dipartimento di Fisica dell'Università, INFN Sezione di Pisa, e Scuola Normale Superiore, I-56010 Pisa, Italy*

G.A. Blair, L.M. Bryant, J.T. Chambers, M.G. Green, T. Medcalf, P. Perrodo, J.A. Strong, J.H. von Wimmersperg-Toeller

*Department of Physics, Royal Holloway & Bedford New College, University of London, Surrey TW20 OEX, United Kingdom*[10]

D.R. Botterill, R.W. Clifft, T.R. Edgecock, S. Haywood, P.R. Norton, J.C. Thompson, A.E. Wright

*Particle Physics Dept., Rutherford Appleton Laboratory, Chilton, Didcot, Oxon OX11 OQX, United Kingdom*[10]

B. Bloch-Devaux, P. Colas, S. Emery, W. Kozanecki, E. Lançon,[2] M.-C. Lemaire, E. Locci, P. Perez, J. Rander, J.-F. Renardy, A. Roussarie, J.-P. Schuller, J. Schwindling, A. Trabelsi, B. Vallage

*CEA, DAPNIA/Service de Physique des Particules, CE-Saclay, F-91191 Gif-sur-Yvette Cedex, France*[17]

S.N. Black, J.H. Dann, R.P. Johnson, H.Y. Kim, N. Konstantinidis, A.M. Litke, M.A. McNeil, G. Taylor

*Institute for Particle Physics, University of California at Santa Cruz, Santa Cruz, CA 95064, USA*[22]

C.N. Booth, S. Cartwright, F. Combley, M.S. Kelly, M. Lehto, L.F. Thompson

*Department of Physics, University of Sheffield, Sheffield S3 7RH, United Kingdom*[10]

K. Affholderbach, A. Böhrer, S. Brandt, G. Cowan, C. Grupen, P. Saraiva, L. Smolik, F. Stephan

*Fachbereich Physik, Universität Siegen, D-57068 Siegen, Germany*[16]

G. Giannini, B. Gobbo, G. Musolino

*Dipartimento di Fisica, Università di Trieste e INFN Sezione di Trieste, I-34127 Trieste, Italy*

J. Rothberg, S. Wasserbaech

*Experimental Elementary Particle Physics, University of Washington, WA 98195 Seattle, U.S.A.*

S.R. Armstrong, A.P. Betteridge, E. Charles, P. Elmer, D.P.S. Ferguson, Y. Gao, S. González, T.C. Greening, O.J. Hayes, H. Hu, S. Jin, P.A. McNamara III, J.M. Nachtman,[23] J. Nielsen, W. Orejudos, Y.B. Pan, Y. Saadi, I.J. Scott, J. Walsh, Sau Lan Wu, X. Wu, G. Zobernig

*Department of Physics, University of Wisconsin, Madison, WI 53706, USA*[11]

[1]Now at CERN, 1211 Geneva 23, Switzerland.
[2]Also at CERN, 1211 Geneva 23, Switzerland.
[3]Also at Dipartimento di Fisica, INFN, Sezione di Catania, Catania, Italy.
[4]Also Istituto di Fisica Generale, Università di Torino, Torino, Italy.
[5]Also Istituto di Cosmo-Geofisica del C.N.R., Torino, Italy.
[6]Supported by the Commission of the European Communities, contract ERBCHBICT941234.
[7]Supported by CICYT, Spain.
[8]Supported by the National Science Foundation of China.
[9]Supported by the Danish Natural Science Research Council.
[10]Supported by the UK Particle Physics and Astronomy Research Council.
[11]Supported by the US Department of Energy, grant DE-FG0295-ER40896.
[12]Permanent address: Kangnung National University, Kangnung, Korea.
[13]Supported by the US Department of Energy, contract DE-FG05-92ER40742.
[14]Supported by the US Department of Energy, contract DE-FC05-85ER250000.
[15]Permanent address: Universitat de Barcelona, 08208 Barcelona, Spain.
[16]Supported by the Bundesministerium für Bildung, Wissenschaft, Forschung und Technologie, Germany.
[17]Supported by the Direction des Sciences de la Matière, C.E.A.
[18]Supported by Fonds zur Förderung der wissenschaftlichen Forschung, Austria.
[19]Also at Istituto di Matematica e Fisica, Università di Sassari, Sassari, Italy.
[20]Now at Harvard University, Cambridge, MA 02138, U.S.A.
[21]Now at University of Geneva, 1211 Geneva 4, Switzerland.
[22]Supported by the US Department of Energy, grant DE-FG03-92ER40689.
[23]Now at University of California at Los Angeles (UCLA), Los Angeles, CA 90024, U.S.A.

# 1 Introduction and method

Charmless semileptonic B meson decays have already been studied in both exclusive and inclusive channels in $\Upsilon(4S)$ decays [1, 2]. From an experimental point of view exclusive searches are somewhat easier because the final states are well constrained, allowing mass peaks to be directly searched for. As a drawback, large theoretical uncertainties affect the transition amplitude, thus leading to model dependent measurements of the CKM matrix element $|V_{ub}|$. For this reason, inclusive measurements have been made, from an excess of events at the endpoint of the lepton momentum distribution where the contribution from $b \to X_c \ell \nu_\ell$ vanishes ($2.3 < p < 2.6$ GeV/$c$). However, from this small region of the lepton phase space, an extrapolation to the low momentum region is needed to extract the value of $|V_{ub}/V_{cb}|$, leading again to a model dependent measurement. In addition, this technique cannot be applied efficiently at LEP since the momentum of the lepton in the b hadron rest frame cannot be reconstructed with sufficient accuracy. Furthermore, this method requires the B flight direction and therefore the B decay vertex to be reconstructed, which introduces different efficiencies for final states $X_u$ with different charged multiplicities.

The model dependence can be reduced if the hadronic system in $b \to X \ell \nu_\ell$ candidates can be analyzed. As shown in Fig. 1, 90% of $b \to X_u \ell \nu_\ell$ decays are expected to have an invariant mass $M_X < 1.87$ GeV/c$^2$, i.e., below charm threshold [3, 4],while only 10% of these decays have a lepton with energy $E_\ell^\star$ above the kinematic boundary for $b \to c$ transitions. This paper presents an inclusive measurement based on the different kinematic properties differentiating $b \to X_u \ell \nu_\ell$ from $b \to X_c \ell \nu_\ell$ decays.

At $\sqrt{s} \sim m_Z$, the two b hadrons produced in $Z \to b\bar{b}$ events are emitted almost back to back in two opposite hemispheres with an average energy of 32 GeV, and their decay products do not mix. This is a favourable situation compared to the $\Upsilon(4S)$ decays where the two b mesons are produced almost at rest. On the other hand, the fragmentation process of a b quark to a b hadron radiates on average 13 GeV divided among several particles, leading to a dilution of the signal. It is therefore a major challenge of the analysis described in this paper to isolate particles from B decays and particles from fragmentation. This separation can only be statistical, thus degrading the resolution on the hadronic mass $M_X$. The information can be retrieved by considering several other variables that keep memory of the kinematics of the decay process.

The following inclusive method based on the different kinematics properties of the $X_u \ell \nu_\ell$ and $X_c \ell \nu_\ell$ final states was therefore developed.

1. All the quantities are measured in the b hadron rest frame. Their determination requires the identification, with good efficiency, of the particles produced in the final state $X \ell \nu_\ell$, and the rejection, with highest possible efficiency, of the particles coming from fragmentation.

2. A set of kinematic variables is built in this frame to discriminate between the $X_u \ell \nu_\ell$ and $X_c \ell \nu_\ell$ transitions, taking advantage of the different properties of these final states. In order to reduce the sensitivity of the measurement to the composition of the $X_u$ hadronic system (i.e., to have similar efficiencies for all final states), both charged particles and photons are used in the evaluation of these variables.

3. To enhance the discriminating power, these variables are combined (here, with a neural network technique). The branching ratio $\mathrm{Br}(b \to X_u \ell \nu_\ell)$ is obtained from a fit

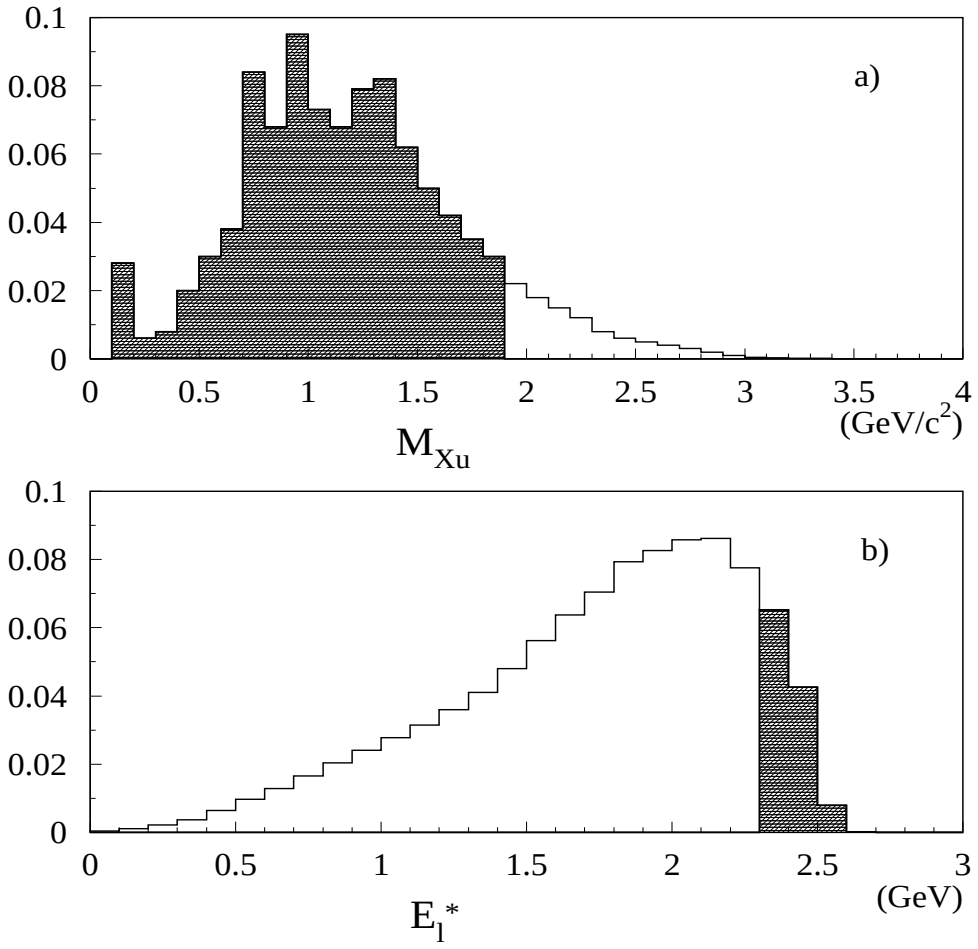


Figure 1: a) Hadronic invariant mass distribution in $b \to X_u \ell \nu_\ell$ decays [4] and b) lepton momentum distribution calculated in the b-hadron rest frame. In the two plots, the shaded area indicates the region inaccessible to $b \to c$ transitions. These two distributions are the predictions of the hybrid model [5] (see Section 4.2 for more details). They do not include smearing effects due to fragmentation particles and detector resolution.

to the part of the neural network output distribution enriched in b $\rightarrow$ u transitions.

Finally, the most recent theoretical results allow the value of $|V_{ub}|$ to be extracted from the inclusive semileptonic branching ratio $Br(b \rightarrow X_u \ell \nu_\ell)$ with an uncertainty of the order of 4% [36].

# 2 The ALEPH detector

The ALEPH detector [6] and its performance [7] are described in detail elsewhere. Only a brief account of the parts of the apparatus relevant for this analysis is given here. Charged particles are detected over the range $|\cos\theta| < 0.95$, by an inner drift chamber (ITC) and a large time projection chamber (TPC), complemented by a silicon strip vertex detector (VDET) made of two layers of radius 6.5 and 11.3 cm and angular coverage $|\cos\theta| < 0.85$ and $|\cos\theta| < 0.69$. The three tracking detectors are immersed in a magnetic field of 1.5 T and together provide a transverse momentum resolution of $\sigma(1/p_T) = 0.6 \times 10^{-3} (\mathrm{GeV}/c)^{-1}$ for high momentum charged particles.

The impact parameter of the tracks of charged particles with momentum in excess of 10 GeV/$c$ and reconstructed with two VDET coordinates is measured by the tracking system with a precision of 35 microns with respect to an event-by-event interaction point. This resolution allows $Z \rightarrow b\bar{b}$ events to be selected by exploiting the longer lifetime of b hadrons with respect to other hadrons, with an algorithm based upon the track impact parameter measurement described in [8].

In addition to its rôle as a tracking device, the TPC also serves to separate charged particle species with up to 338 measurements of their specific ionization, $dE/dx$. It allows electrons to be separated from pions by more than three standardro deviations up to a momentum of 8 GeV/$c$.

The electromagnetic calorimeter (ECAL), which surrounds the tracking detectors inside the superconducting solenoid, is used, together with the TPC, to identify electrons and photons from the characteristic longitudinal and transverse profiles of their associated showers [7]. It consists of 45 layers of lead interleaved with proportional wire chambers, and covers the angular region $|\cos\theta| < 0.98$. The relative energy resolution achieved for isolated electromagnetic showers is $0.18/\sqrt{E}$ ($E$ in GeV).

Muons are identified by their penetration pattern in the hadron calorimeter, composed of the iron of the magnet return yoke interleaved with 23 layers of streamer tubes, and by muon chambers made of two layers of streamer tubes surrounding the calorimeter.

Typical identification efficiencies of 65% and 85% are obtained for electrons and muons while the hadron misidentification probabilities are respectively of the order of 0.1% and 1% [9].

The total visible energy is measured with the energy-flow reconstruction algorithm described in [7]. This algorithm also provides a list of charged and neutral reconstructed objects, called *energy-flow particles* in the following.

# 3 Selection and reconstruction of the b hadron

Hadronic Z decays are selected following the method described in [10]. A total of 3.6 million events are selected during the period 1992 to 1995. Each event is divided into two

hemispheres using the plane perpendicular to the thrust axis, and the polar angle of this axis is required to satisfy $|\cos\theta_{\rm thrust}| < 0.7$.

Candidate $b \to X_u \ell \nu_\ell$ events are selected and the boost of the b hadron reconstructed as follows.

- At least one identified lepton with $p > 3$ GeV/$c$ is required.
- The b lifetime tag [8] is applied to the hemisphere opposite to the lepton candidate. This selects about 25% of the b hemispheres, while reducing the non-b contamination to less than 2%. The sample obtained contains 47 672 hemispheres of which 19 803 have an electron candidate and 27 869 a muon candidate.
- The three-momentum vector $\vec{p}_\nu$ of the neutrino is estimated from the missing momentum of the lepton hemisphere [11], the visible energy being computed with all the energy-flow particles. Typical resolutions on the neutrino direction of 280 mrad and of 2 GeV on its energy are obtained.
- The selection of the particles originating from the hadronic system X is performed using two neural networks, one to select photons and the other charged particles. Neutral hadronic energy flow particles ($K^0_L$, neutrons, ...) are not used here since they contribute only 4% of the energy of the hadronic system in $b \to u$ transitions, while 14% in the fragmentation process. The choice of the input variables, listed in the Appendix, is based on the fact that particles from b decays are more energetic, closer to the lepton and to their nucleated jet axis (see the Appendix for the definition of this axis) than particles from fragmentation and do not originate from the primary vertex of the event. The outputs $NN_\gamma$ for photons and $NN_c$ for charged particles are shown in Fig. 2 for simulated particles from fragmentation and from b hadron decays. The separation is better for charged particles than for photons due to the use of the track impact parameter. Figure 3 shows the comparison between data and Monte Carlo. A discrepancy of 20% can be seen at low values of $NN_\gamma$ where the contribution of photons from fragmentation is dominant. The disagreement is mainly due to inaccuracies in the simulation of low energy photons and neutral hadrons, which are more numerous in the Monte Carlo than in the data. This effect is corrected by removing 20% of photons from fragmentation in the simulation, Fig. 3c. A cut on $NN_c$ and $NN_\gamma$ (Fig. 2) allows particles coming from the hadronic system X to be selected with an efficiency of 85% and purities of 80% and 75% for $b \to c$ and $b \to u$ transitions, respectively. Other clustering algorithms were used as a check of which the best one was found to be "BTCONE" [12], giving a 10% worse purity for the same efficiency. The systematic effects related to the choice of clustering algorithm are studied in Section 8.4.

The b hadron rest frame is then reconstructed by adding the momenta of the lepton, the neutrino and the selected particles. The total energy is determined by assigning a mass of 5.38 GeV/$c^2$ to the total system. The average value of the reconstructed b energy is 32.18 GeV for the data and 32.05 GeV in the simulation, with 58% coming from charged particles, 17% from photons and 25% from the neutrino. The momentum and angular resolutions, obtained from the simulation, are respectively 4.5 GeV/$c$ and 60 mrad.

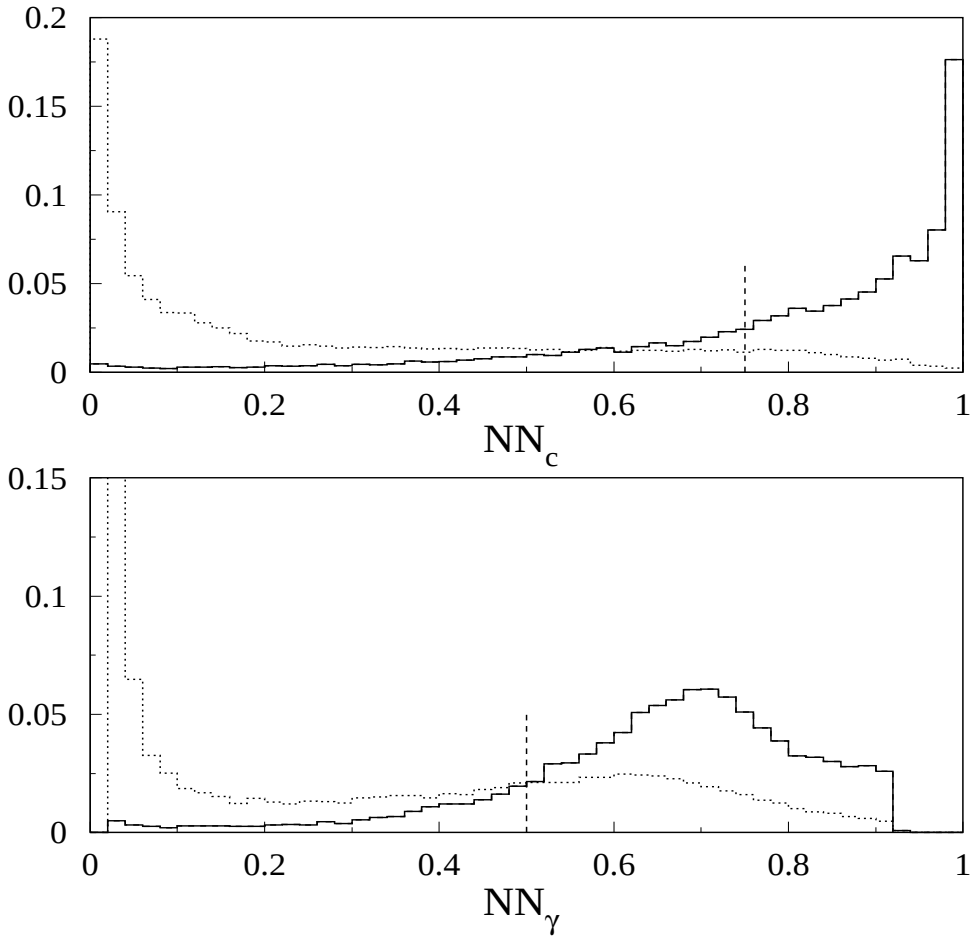


Figure 2: Neural network output for charged particles (upper plot) and photons (lower plot). The solid histogram is for tracks coming from B decays (with 1% of $b \to u$ transitions) and the dotted one is for tracks produced in the fragmentation. The two Monte Carlo distributions are normalized to the same area. The dashed vertical lines indicate the cuts used in the analysis.

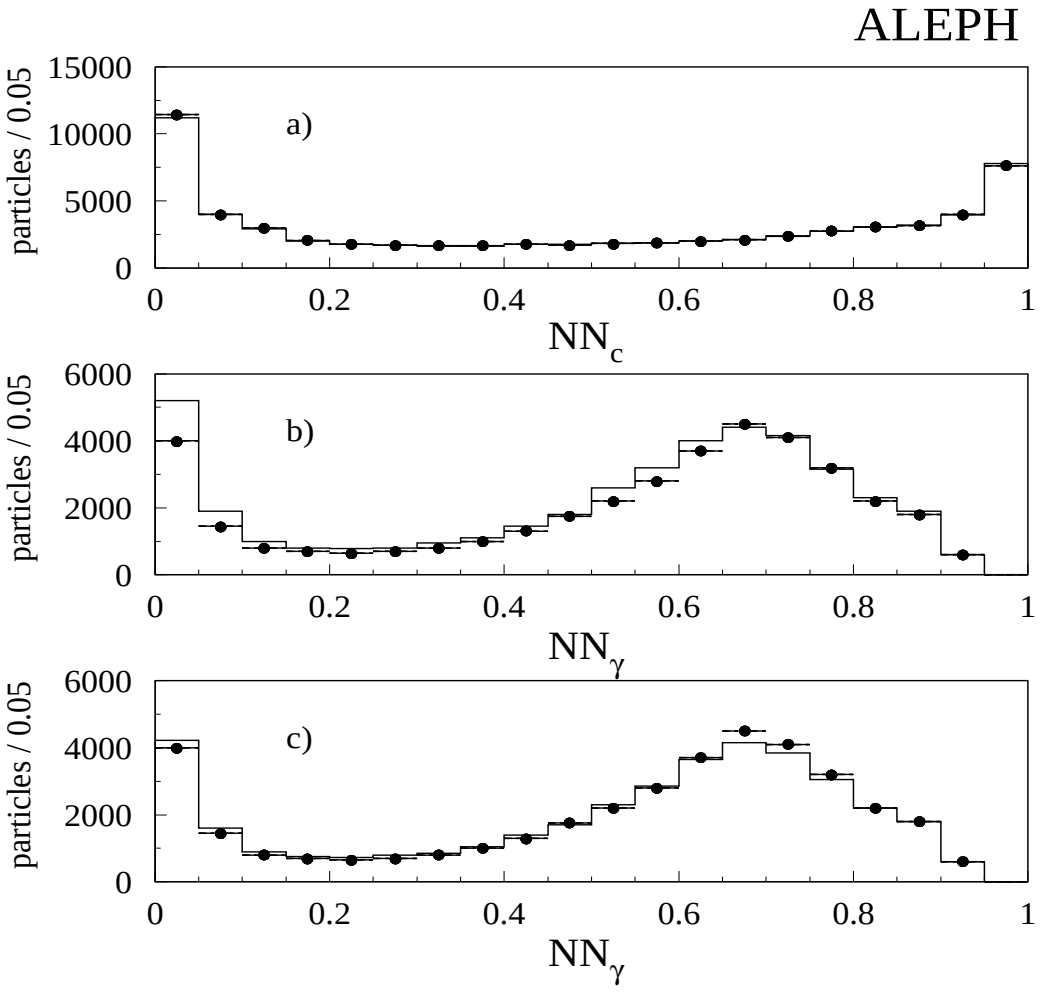


Figure 3: Comparison between data (points) and Monte Carlo (histogram) for: a) $NN_c$, b) $NN_\gamma$ without correction on photons from fragmentation and c) $NN_\gamma$ with correction.

# 4 Simulation of semileptonic decays of b hadrons

## 4.1 Simulation of b $\rightarrow$ c transitions

Samples of 4.5 million $Z \rightarrow q\bar{q}$ events and 1.5 million $Z \rightarrow b\bar{b}$ events were simulated with a generator based on the JETSET 7.4 parton shower model [13]. The following corrections were applied according to the most recent measurements [14].

1. The decay properties of the $D^+$, $D^0$, $D_s^+$ mesons and of the $\Lambda_c$ baryons were modified to reproduce those given by the MARKIII Collaboration [15] and the Particle Data Group [16]. This includes the exclusive branching ratios, the inclusive production rates of $\pi^0$, $K^0$, $\bar{K}^0$, $K^\pm$, p, $\Lambda$ and the topological branching ratios (i.e., branching ratios $B_i$, where $B_i$ applies for final states containing i charged particles).

2. The modelling of the lepton momentum distribution in the $b \rightarrow X_c \ell \nu_\ell$ transitions is done with the predictions of the ACCMM [17] model fitted on the CLEO data [18]. This corresponds to a fraction of $D^{**}$ and nonresonant $D\pi + D^*\pi$ (produced with equal rates) of 18% with respect to all $X_c$ hadronic final states.

3. The $c \rightarrow \ell$ spectrum is obtained by reweighting the energy spectrum given by JETSET in the centre-of-mass system of the decaying c hadron so that it reproduces the DELCO [19] and MARKIII [20] data combined.

4. The $b \rightarrow c \rightarrow \ell$ momentum spectrum is obtained with the previous corrections for the $c \rightarrow \ell$ part and the CLEO data [21] for the $B \rightarrow D$ part.

5. The values of $Br(b \rightarrow X_c \ell \nu_\ell)$, $Br(b \rightarrow c \rightarrow \ell)$ and of the b fragmentation parameter $\langle X_b \rangle$ are taken from the ALEPH analysis of the lepton $p$ and $p_\perp$ distributions [22]:

$$\begin{aligned} Br(b \rightarrow X_c \ell \nu_\ell) &= (11.03 \pm 0.07_{stat} \pm 0.30_{syst})\%, \\ Br(b \rightarrow c \rightarrow \ell) &= (7.83 \pm 0.12_{stat} \pm 0.49_{syst})\%, \\ \langle X_b \rangle &= 0.708 \pm 0.003_{stat} \pm 0.010_{syst} \ . \end{aligned}$$

   The related systematics will be discussed in Section 7.1.

## 4.2 Simulation of b $\rightarrow X_u \ell \nu_\ell$ transitions

A total of 50,000 $b \rightarrow X_u \ell \nu_\ell$ transitions (about 15 times the number of events expected) has been simulated using the hybrid model described in Ref. [5]. At low hadronic energy (below 1.6 GeV), only resonant final states are produced, while for large energy, nonresonant multi-pion final states are expected to dominate. The choice of the cutoff $\Lambda$ used to define the two regions is based on an analogy between the hadronic final states found in semileptonic B decays and the corresponding final states produced in ep scattering. This model predicts that the nonresonant states represent 75% of the $b \rightarrow X_u \ell \nu_\ell$ transitions for a cutoff value of 1.6 GeV.

In the bound states region ($\Lambda < 1.6$ GeV), the predictions of the ISGW2 model [23] are used. With this value of $\Lambda$, the pseudoscalar, vector and heavy (1S, 2S and 1P) states represent respectively 17%, 46% and 37% of the resonant states.

In the nonresonant region ($\Lambda \geq 1.6$ GeV), the inclusive model of Dikeman, Shifman and Uraltsev (called DSU in the following) is used to predict the invariant mass distribution of the hadronic system X, the momentum transfer ($q^2$) distribution of the virtual W and the lepton momentum spectrum [24]. This model is based on the Heavy Quark Expansion theory and has been already used to describe the $b \to s\gamma$ transitions. It depends on two parameters, the mass $m_b$ of the b quark as determined in Ref. [25] and the kinetic energy operator $\mu_\pi^2$ of the b quark in the b hadron estimated by the QCD sum rules to be $(0.4 \pm 0.2)$ GeV$^2$ [26]. The dependence on $\mu_\pi^2$ and $m_b$ of the lepton momentum distribution, $q^2$ and the invariant mass of the hadronic system $X_u$ is shown in Ref. [3].

Systematics related to this simulation are described in Section 7.2.

# 5 Discrimination between $b \to c$ and $b \to X_u \ell \nu_\ell$ transitions

The discrimination between the $b \to X_u \ell \nu_\ell$ signal decays and the background from $b \to c$ transitions is based on the fact that the c quark is heavy compared to the u quark, leading to different kinematic properties for the two final states. Because of resolution effects, this separation cannot be optimal with a single kinematic variable such as $M_X$ and is considerably improved by combining in a multivariate analysis informations characterizing the leptonic part and the hadronic part. To take into account the correlations between the different variables, a neural network is used here, the output of which is called $NN_{bu}$ in the following.

The quantities used to build the input variables are: sphericities, multiplicities, energies, invariant masses, the momenta and transverse momenta of particles, etc. All these quantities are defined from the particles selected with $NN_c$ and $NN_\gamma$ and computed in the reconstructed b hadron rest frame. The choice of the input variables is based on the following requirements:

1. A good discrimination between $b \to X_u \ell \nu_\ell$ and $b \to X_c \ell \nu_\ell$.

2. A reduced sensitivity to the composition of the $X_u$ system (for instance, no vertexing is used to build the input variables of $NN_{bu}$).

In addition, a good agreement between data and simulation for the selected variables and for their correlations is required. This led to a set of 20 variables (listed in Appendix) used as inputs of a 20-15-10-1 multi-layered neural network. The discrimination between signal and background and the comparison between data and Monte Carlo are shown in Fig. 4 and Fig. 5 for four of the 20 variables. A similar agreement between data and Monte Carlo is observed for the other variables. The neural network output obtained with simulated $Z \to b\bar{b}$ events is shown in Fig. 6 for $b \to X_u \ell \nu_\ell$ events and $b \to X_c \ell \nu_\ell$ background events. Although a better separation than with each individual variable is achieved, a significant background remains in the signal region of high $NN_{bu}$ and is the main source of systematic uncertainty in the analysis (see Section 7). Figure 7 shows a breakdown of the background into its main components. As expected, the largest contamination in the signal region is from $X_c = D$ or $D^*$. For heavier states such as $D^{**}$ or nonresonant $D^*\pi$ systems, and for cascade decays where the lepton is less energetic, the contamination is smaller. Figures 8 and 9 display the components of the signal showing that the neural network output is

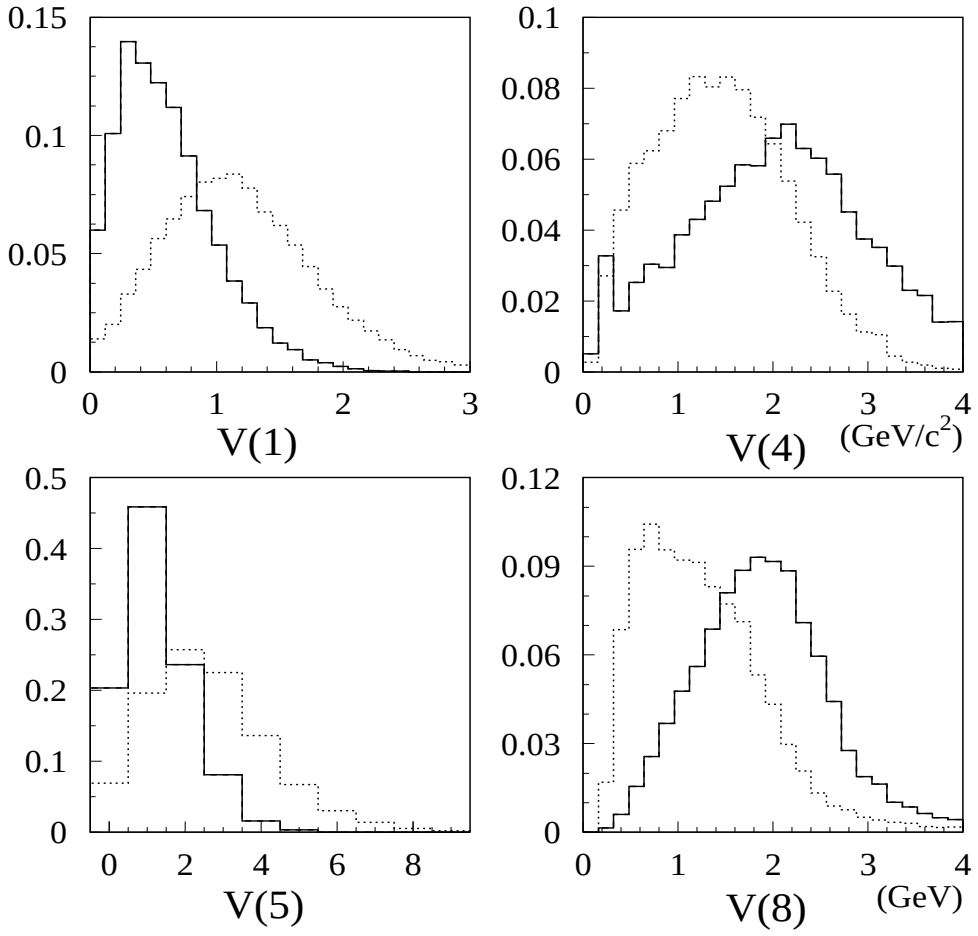


Figure 4: Comparison between signal transitions $b \to X_u \ell \nu_\ell$ (solid lines) and background $b \to c$ transitions (dotted lines) for four variables used as input of $NN_{bu}$: $V(1) = [\sum_j (\sum_{i \leq j} p_\perp(i))(\sum_{i \leq j} p_{//}(i))]/[\sum_j p(j)]^2$ where $p_\perp(i)$ and $p_{//}(i)$ refer to the transverse and longitudinal momenta of the particles i of the lepton hemisphere, ordered by decreasing energy values. V(4) is the invariant mass of the two most energetic particles, V(5) is the charged particle multiplicity and V(8) is the energy of the lepton in the reconstructed b hadron rest frame. The particles which enter in the definition of these variables have to satisfy the cuts on $NN_c$ or $NN_\gamma$ (see Section 3). The two reconstructed Monte Carlo distributions are normalized to the same area.

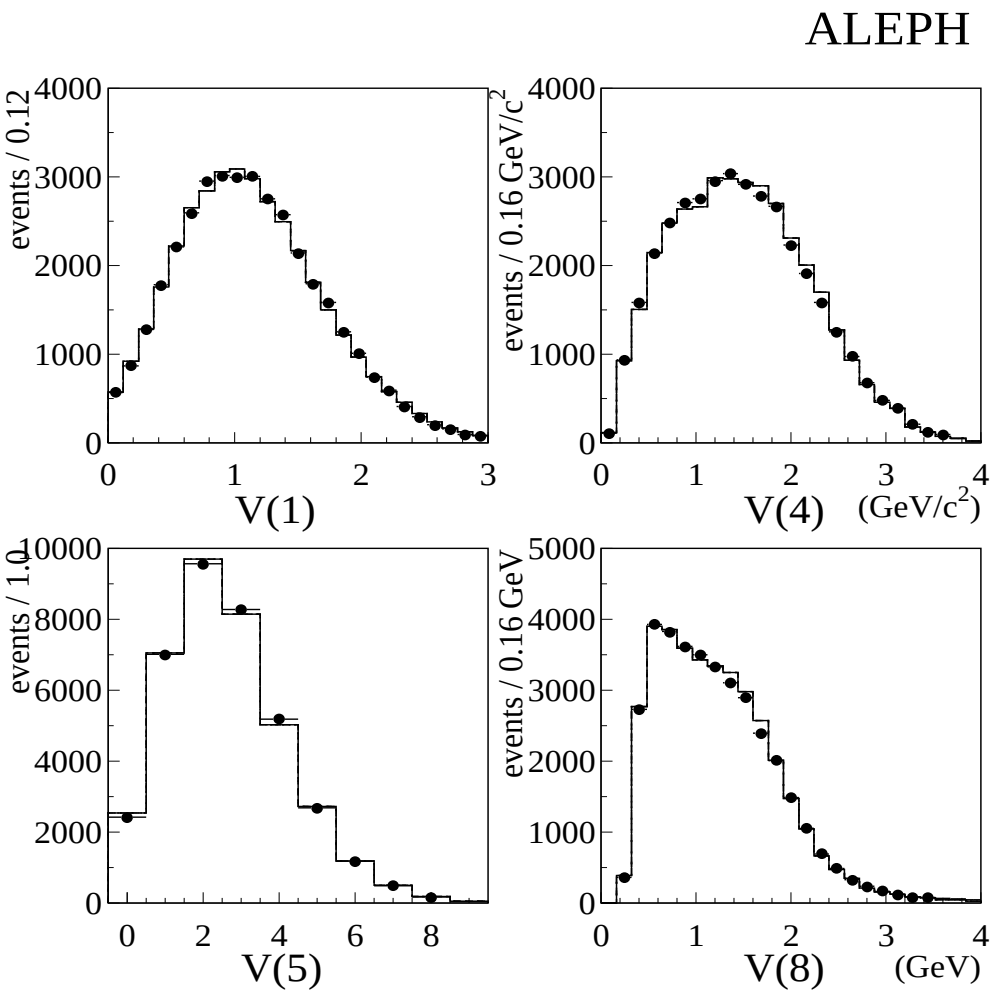


Figure 5: Comparison between data (points) and Monte Carlo (histogram) for the four input variables of figure 4.

similar for all the resonant states except $2^+$ and $1^+$ non strange resonances [16] (denoted f + a + b in the following) and that charged and neutral states (like $\rho^0$ and $\rho^\pm$) are comparable. The corresponding acceptances are given in Table 1 for $NN_{bu} \geq 0.6$ and $NN_{bu} \geq 0.8$. The related systematics are discussed in Section 7.2.

Table 1: Acceptances of the simulated b → u transitions shown in Fig. 8 for two cuts on $NN_{bu}$.

| Acceptance (%) | $\pi^0$ | $\pi^+$ | $\eta + \eta'$ | $\rho^0$ | $\rho^+$ | $\omega$ | f + a + b | K + K* | nπ |
|---|---|---|---|---|---|---|---|---|---|
| $NN_{bu} \geq 0.6$ | 78 | 69 | 58 | 52 | 67 | 49 | 43 | 67 | 49 |
| $NN_{bu} \geq 0.8$ | 48 | 40 | 27 | 20 | 31 | 17 | 15 | 34 | 24 |

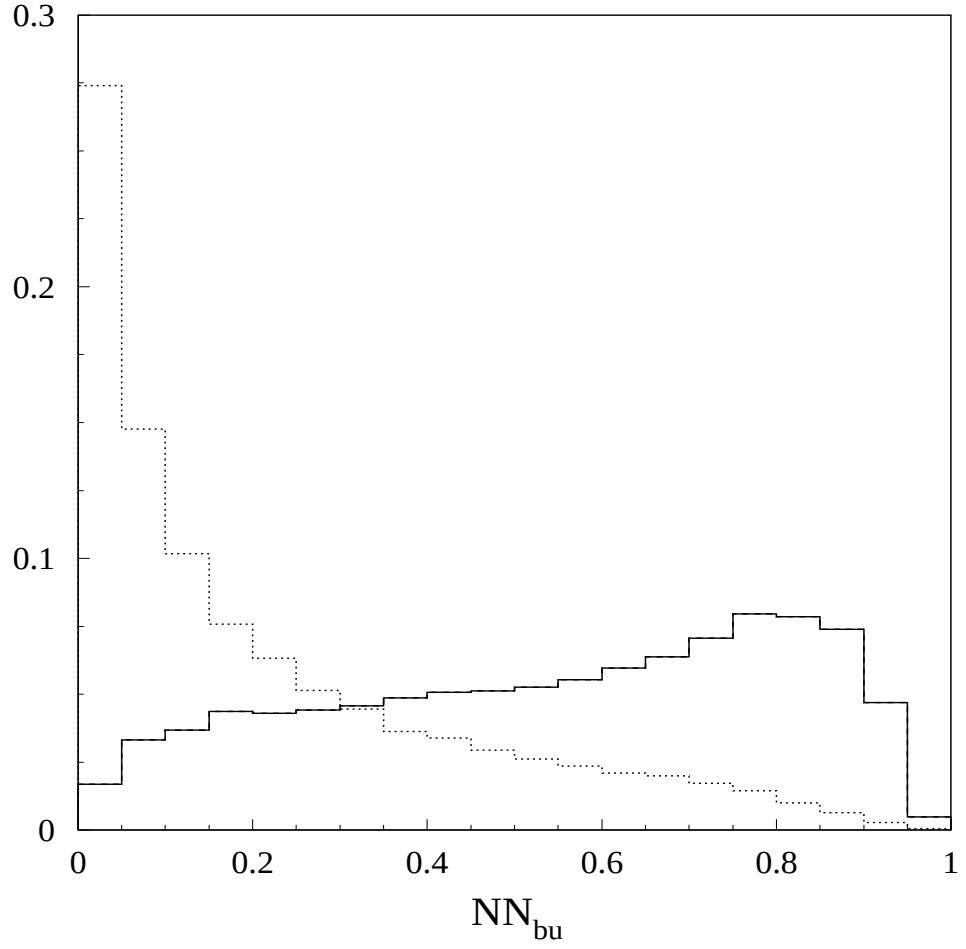


Figure 6: Output of $NN_{bu}$ for signal b → $X_u \ell \nu_\ell$ transitions (solid lines) and background b → c transitions (dotted lines). The two Monte Carlo distributions are normalized to the same area.

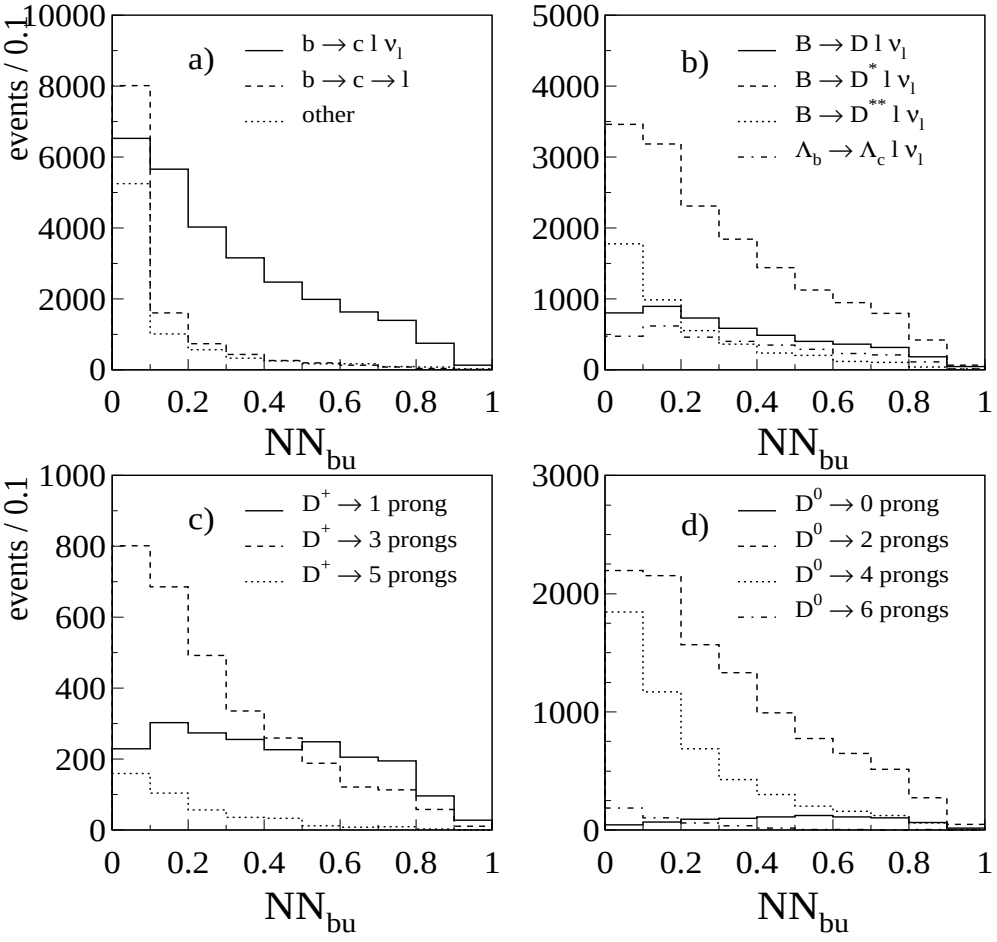


Figure 7: Breakdown of the b → c background into its main components. a) Comparison between direct b → c$\ell\nu_\ell$ and casdade b → c → $\ell$ transitions; b) comparison between different hadronic final states $X_c$; c) and d) comparison of topological final states in $D^+$ and $D^0$ decays respectively. The histograms are normalized to the number of entries in the data.

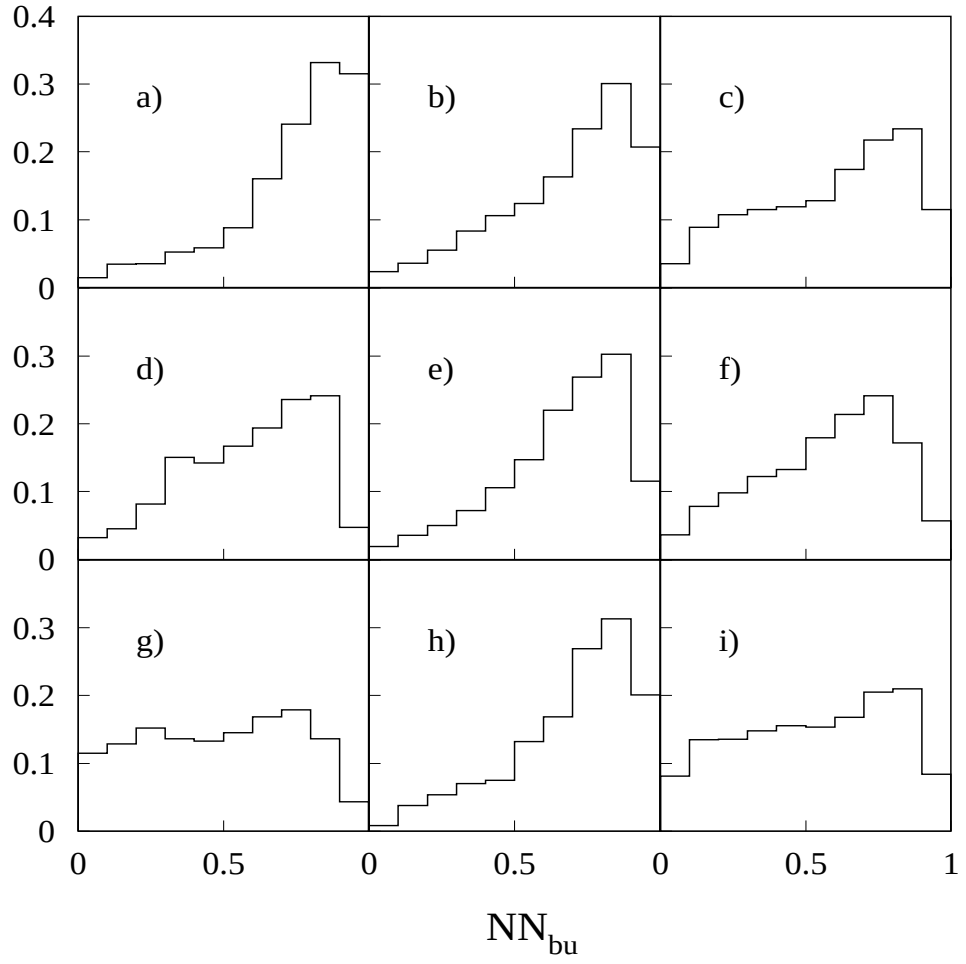


Figure 8: Output of $NN_{bu}$ for simulated $b \to X_u \ell \nu_\ell$ transitions: a) $B \to \pi^0 \ell \nu_\ell$, b) $B \to \pi^+ \ell \nu_\ell$, c) $B \to (\eta + \eta^{'}) \ell \nu_\ell$, d) $B \to \rho^0 \ell \nu_\ell$, e) $B \to \rho^+ \ell \nu_\ell$, f) $B \to \omega \ell \nu_\ell$, g) $B \to (f + a + b) \ell \nu_\ell$, h) $B \to (K + K^*) \ell \nu_\ell$ and i) $B \to (n\pi) \ell \nu_\ell$. The different contributions are normalized to the same area.

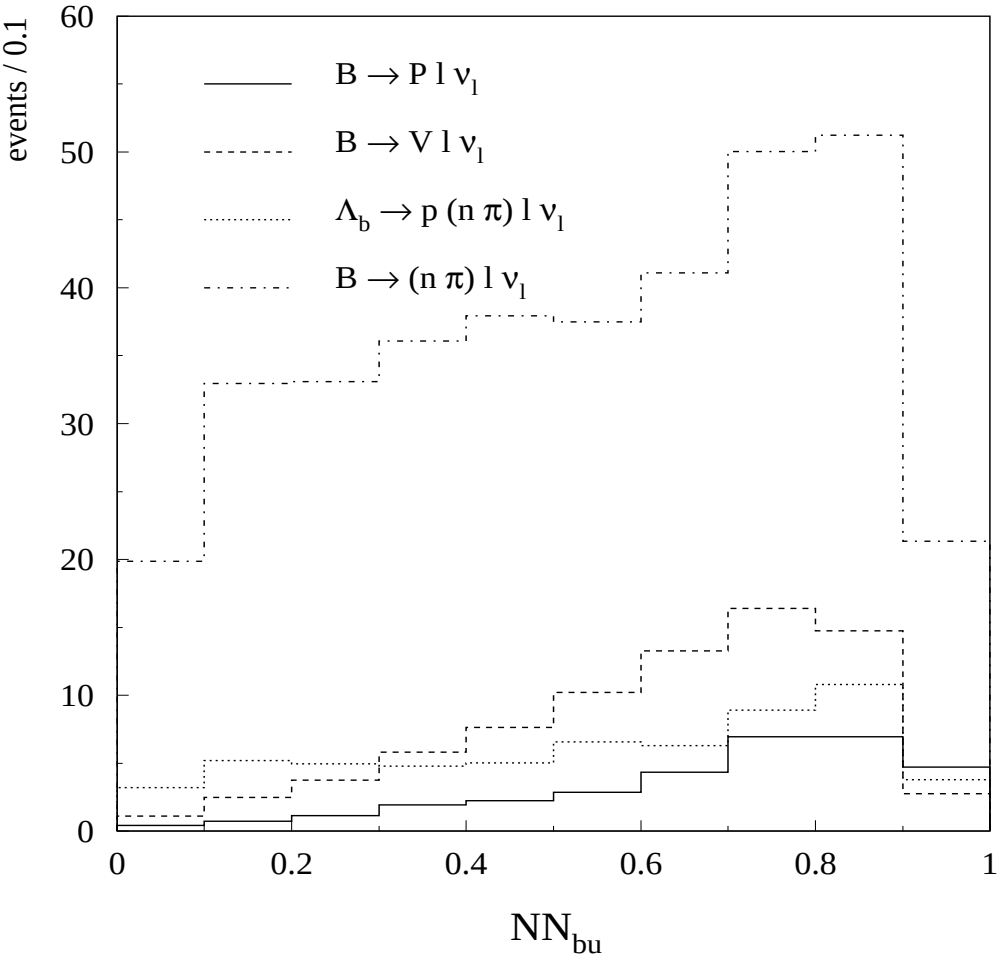


Figure 9: Breakdown of the $b \to X_u \ell \nu_\ell$ contribution into resonant pseudoscalar (P) and vector (V) states, nonresonant b meson decays and $\Lambda_b$ decays. The histograms are normalized to the number of entries in the data.

# 6 Result

Figure 10 shows the $NN_{bu}$ distribution for the Monte Carlo and data after all the selection cuts. The histogram for the Monte Carlo is subdivided into the contributions from $b \to X_u \ell \nu_\ell$, $b \to X_c \ell \nu_\ell$, $b \to c \to \ell$ decays and from other sources. Table 2 gives the number of entries in each bin of Fig. 10 for each of these sources. The number of entries given for $b \to X_u \ell \nu_\ell$ corresponds to the measured branching ratio obtained below. The Monte Carlo is normalized to have the same number of entries as the data when calculating the $b \to X_u \ell \nu_\ell$ branching ratio, as this reduces sensitivity to the assumed efficiencies of the analysis cuts. Furthermore, the first bin of the $NN_{bu}$ distribution is excluded in this normalization process as this minimizes the effects of the uncertainties of background events, such as $b \to D^{**} \ell \nu_\ell$ and $b \to c \to \ell$, in the fit. The influence of this procedure on the systematic errors is discussed in Section 7.1. The branching ratio is then fitted from the data in the following way. A likelihood is calculated, summed over the bins of Fig. 10 with $NN_{bu} > NN_{cut}$, where the likelihood in each bin is defined as

$$-\ln \mathcal{L}_k = \frac{[N_k^{data} - (\alpha N_k^{MC_{b\to u}} + \beta N_k^{MC_{b\to c}})]^2}{2N_k^{data}} + \frac{1}{2}\ln(2\pi N_k^{data}) \,,$$

where $\alpha$ is the free parameter of the fit and $\beta$ is the coefficient used to normalize data and Monte Carlo to the same number of entries:

$$\beta = \frac{\sum_j (N_j^{data} - \alpha N_j^{MC_{b\to u}})}{\sum_j N_j^{MC_{b\to c}}} \,.$$

In the calculation of the normalization parameter $\beta$, the sums run over the bins with $NN_{bu} > 0.1$. Finally, the measured branching ratio is defined as $Br(b \to X_u \ell \nu_\ell) = \alpha \times Br^{MC}(b \to X_u \ell \nu_\ell)$, where $Br^{MC}(b \to X_u \ell \nu_\ell)$ is the value used as input in the simulation. The value $NN_{cut} = 0.6$ has been chosen as it leads to the smallest total relative error (see Fig. 15). This corresponds to an efficiency of 50% for the signal. Good agreement is observed between data and Monte Carlo in the $b \to c$ region (i.e., $NN_{bu} < 0.6$) while there is an excess of $(303 \pm 88)$ events in the signal region which is compatible both in rate and in shape with signal $b \to X_u \ell \nu_\ell$ transitions. The result of the fit is

$$Br(b \to X_u \ell \nu_\ell) = (1.73 \pm 0.55_{stat}) \times 10^{-3},$$

where the statistical error has a $\pm 0.48 \times 10^{-3}$ contribution from the data and $\pm 0.28 \times 10^{-3}$ from the limited Monte Carlo statistics. If the fit is done separately for electrons and muons, the results are respectively $(1.1 \pm 0.8_{stat}) \times 10^{-3}$ and $(2.3 \pm 0.8_{stat}) \times 10^{-3}$.

# 7 Studies of systematic uncertainties

The uncertainties have two origins: the errors associated to the $b \to c$ transitions and those due to the modelling of the $b \to u$ transitions. All these errors are summarized in Table 3.

Table 2: Number of entries in Fig. 10. The Monte Carlo numbers are scaled so as to correspond to a $b \to X_u \ell \nu_\ell$ branching ratio of 0.17% and they have been normalized to have the same total number of entries as the data in the region $NN_{bu} > 0.1$. See the text for more details.

| Source | 0.0-0.1 | 0.1-0.2 | 0.2-0.3 | 0.3-0.4 | 0.4-0.5 | 0.5-0.6 | 0.6-0.7 | 0.7-0.8 | 0.8-0.9 | 0.9-1.0 |
|---|---|---|---|---|---|---|---|---|---|---|
| Data | 20088 | 8199 | 5406 | 3831 | 3070 | 2365 | 1999 | 1597 | 925 | 192 |
| $b \to X_c \ell \nu_\ell$ | 6503 | 5521 | 4120 | 3103 | 2489 | 1938 | 1596 | 1355 | 739 | 123 |
| $b \to c \to \ell$ | 8026 | 1594 | 727 | 422 | 255 | 186 | 126 | 72 | 32 | 9 |
| "others" | 5387 | 1026 | 569 | 303 | 238 | 170 | 165 | 86 | 83 | 24 |
| $b \to X_u \ell \nu_\ell$ | 24 | 40 | 44 | 48 | 55 | 56 | 69 | 81 | 84 | 35 |
| Data $- MC_{b\to c}$ | $172 \pm 162$ | $58 \pm 104$ | $-10 \pm 84$ | $3 \pm 71$ | $88 \pm 63$ | $71 \pm 56$ | $112 \pm 51$ | $84 \pm 46$ | $71 \pm 32$ | $36 \pm 15$ |
| Data $- MC_{b\to c+b\to u}$ | $148 \pm 162$ | $18 \pm 104$ | $-54 \pm 84$ | $-45 \pm 71$ | $33 \pm 63$ | $15 \pm 56$ | $44 \pm 51$ | $3 \pm 46$ | $-13 \pm 32$ | $1 \pm 15$ |
| | Breakdown of the $b \to X_c \ell \nu_\ell$ contribution in term of charmed topological final states | | | | | | | | | |
| $D \to 1$ prong | 354 | 456 | 422 | 385 | 359 | 368 | 319 | 280 | 151 | 34 |
| Rest | 6149 | 5065 | 3698 | 2718 | 2130 | 1570 | 1277 | 1075 | 588 | 89 |
| | Contribution of the $D^{**}$ to $b \to X_c \ell \nu_\ell$ | | | | | | | | | |
| $b \to (D^{**} + D^* \pi) \ell \nu_\ell$ | 1989 | 1106 | 617 | 404 | 260 | 227 | 147 | 117 | 44 | 10 |
| Rest | 4514 | 4415 | 3503 | 2699 | 2229 | 1711 | 1449 | 1238 | 695 | 113 |
| | Contributions of $e^\pm$ and $\mu^\pm$ to "others" | | | | | | | | | |
| $e^\pm$ | 1387 | 295 | 182 | 78 | 78 | 58 | 47 | 29 | 17 | 5 |
| $\mu^\pm$ | 4000 | 731 | 387 | 225 | 160 | 112 | 118 | 57 | 66 | 19 |
| | Contribution of $Z \to c\bar{c}$ events to "others" | | | | | | | | | |
| $Z \to c\bar{c}$ | 231 | 120 | 70 | 46 | 40 | 14 | 16 | 15 | 4 | 1 |
| Rest | 5117 | 906 | 498 | 257 | 198 | 155 | 148 | 71 | 79 | 23 |

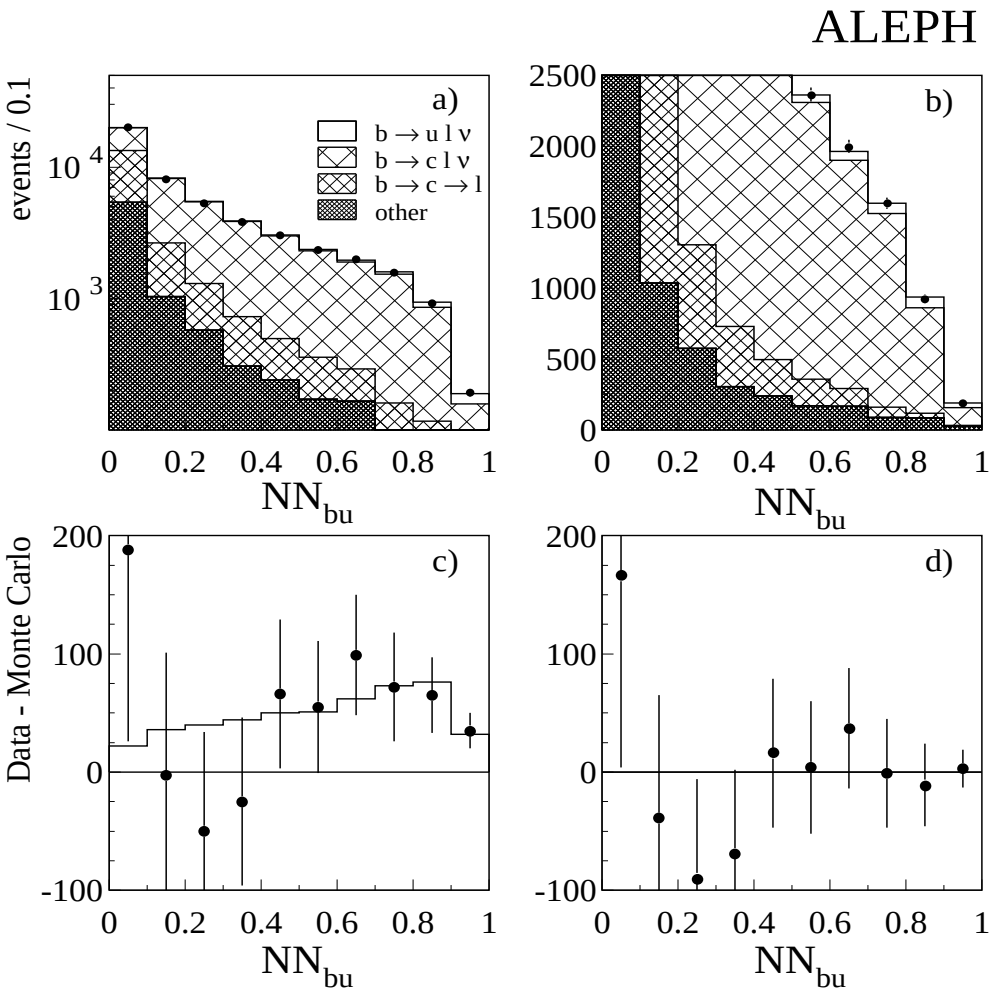


Figure 10: Neural network output $NN_{bu}$: a) and b) comparison between data (points) and Monte Carlo (histogram), c) difference between data and Monte Carlo with no $b \to u$ transitions (points) compared to the $b \to u$ contribution (histogram), and d) difference between data and Monte Carlo with the fitted value of $b \to u$.

Table 3: Estimated contributions to the systematic uncertainty on $\mathrm{Br}(\mathrm{b} \to \mathrm{X_u}\ell\nu_\ell)$. The final total error has been symmetrized.

| Source | Variation | $\Delta\mathrm{Br}(\mathrm{b} \to \mathrm{X_u}\ell\nu_\ell)$ $(10^{-3})$ |
|---|---|---|
| Photons from fragmentation | $\pm 10\%$ | $\mp 0.12$ |
| Boost of the b hadron | (see text) | $\pm 0.07$ |
| $\mathrm{B_s}$ production rate | $(11.2 \pm 1.9)\%$ | $\mp 0.01$ |
| $\Lambda_\mathrm{b}$ production rate | $(11.3 \pm 2.3)\%$ | $\mp 0.07$ |
| $\Lambda_\mathrm{b}$ polarization | $(-30 \pm 30)\%$ | $\mp 0.01$ |
| $\epsilon_\mathrm{c}^{\mathrm{lifetime}}$ | $\pm 13\%$ | $\pm 0.02$ |
| $\sigma_{\mathrm{stat}}^{\mathrm{b}\to\mathrm{c}}$ | (see text) | $\pm 0.22$ |
| $\mathrm{b} \to \ell$ modelling | 28% of $\mathrm{D^{**}}$<br>8% of $\mathrm{D^{**}}$ | $^{+0.06}_{-0.16}$ |
| $\mathrm{D^{**}/(D^*\pi)}$ | $1.0 \pm 0.5$ | $^{-0.03}_{+0.05}$ |
| 4-body rate in $\Lambda_\mathrm{b}$ SL decays | $(20 \pm 20)\%$ | $\pm 0.12$ |
| $\mathrm{B} \to \mathrm{D}$ modelling | (see Ref. [14]) | $\mp 0.04$ |
| $\mathrm{c} \to \ell$ modelling | (see Ref. [14]) | $\pm 0.14$ |
| $\mathrm{Br}(\mathrm{b} \to \psi \to \ell)$ | $\pm 14\%$ | $\mp 0.01$ |
| $\mathrm{Br}(\mathrm{b} \to \tau \to \ell)$ | $\pm 18\%$ | $\pm 0.00$ |
| $\mathrm{Br}(\mathrm{b} \to \bar{\mathrm{c}} \to \ell)$ | $\pm 50\%$ | $\pm 0.00$ |
| c hadron topological B.R. | (see text) | $\pm 0.34$ |
| no. of neutrals in c decays | (see Ref. [16]) | $\pm 0.11$ |
| $\mathrm{D} \to \mathrm{K_L^0 X}$ | (see Ref. [15]) | $\pm 0.08$ |
| $\mathrm{D^0/D^+}$ | $2.59 \pm 0.52$ | $\mp 0.04$ |
| $\Lambda_\mathrm{c} \to \mathrm{nX}$ | $0.50 \pm 0.16$ | $\mp 0.07$ |
| Electron ID efficiency | $\pm 2\%$ | $\mp 0.03$ |
| Photon conversions | $\pm 10\%$ | $\pm 0.00$ |
| Electron background | $\pm 10\%$ | $\pm 0.00$ |
| Muon ID efficiency | $\pm 2\%$ | $\mp 0.05$ |
| Decaying hadrons | $\pm 10\%$ | $\pm 0.00$ |
| Punch-through | $\pm 20\%$ | $\mp 0.04$ |
| Punch + decays shape | | $\pm 0.04$ |
| Total $\mathrm{b} \to \mathrm{c}$ systematic uncertainty | | $\pm 0.51$ |
| Value of the cutoff $\Lambda$ | $0\ \mathrm{GeV} \to \infty$ | $^{+0.06}_{-0.10}$ |
| Exclusive model | JETSET | $\pm 0.05$ |
| Inclusive model | ACCMM<br>Parton model | $\pm 0.18$ |
| $\Lambda_\mathrm{b}$ modelling | (see text) | $\pm 0.04$ |
| Total $\mathrm{b} \to \mathrm{u}$ systematic uncertainty | | $\pm 0.21$ |
| Total systematic uncertainty | | $\pm 0.55$ |

## 7.1 $b \to c$ transitions

The systematic uncertainties associated to the background arise from the limited knowledge of the fragmentation process, the relative production rates of b hadrons, their decays and those of the c hadrons produced from these decays.

### 7.1.1 The fragmentation process

The disagreement observed between data and Monte Carlo in the fragmentation region of the $NN_\gamma$ distribution was taken into account by reweighting the events in the simulation so that the number of photons from fragmentation is varied by $\pm 10\%$. Since more than 80% of photons from fragmentation have an energy smaller than 2 GeV, no attempt for an energy dependent correction was made. The track impact parameter distribution which plays a major rôle in $NN_c$ is corrected as in Ref. [27] and no systematic uncertainty is assigned.

### 7.1.2 Production of b hadrons

The distribution of the b hadron reconstructed boost (as well as its mean value) shows a slight disagreement between Monte Carlo and data. The Monte Carlo events were therefore reweighted so that this distribution matches the observed one, and the analysis was repeated. The difference between the two $Br(b \to X_u \ell \nu_\ell)$ values obtained with and without this correction was taken as the systematic.

The systematic uncertainties associated with the $\Lambda_b$ production were also investigated. First, the fraction of $\Lambda_b$ baryons [28] was varied because the shape of the $NN_{bu}$ distribution differs from that of the B mesons. The shape of the $NN_{bu}$ distribution associated with $B_s$ mesons is very similar to that of $B_u$ and $B_d$, and a variation of the fraction of $B_s$ mesons therefore gives a negligible error on $Br(b \to X_u \ell \nu_\ell)$ [16]. The momentum distributions of the lepton and the neutrino were modified according to the measured value of the $\Lambda_b$ polarization [29].

The small residual contamination from $Z \to c\bar{c}$ events in the selected lepton sample is governed by the efficiency $\epsilon_c^{\text{lifetime}}$ of the lifetime algorithm for such events. The relative error $\Delta\epsilon_c^{\text{lifetime}}/\epsilon_c^{\text{lifetime}}$ on this efficiency is estimated to be $\pm 13\%$ [8], giving a negligible error on $Br(b \to X_u \ell \nu_\ell)$ due to the high purity of $Z \to b\bar{b}$ events in the selected sample.

### 7.1.3 Decay properties of b hadrons

The systematic error $\sigma_{\text{stat}}^{b \to c}$ on $Br(b \to X_u \ell \nu_\ell)$ arising from the statistical uncertainties on $Br(b \to \ell)$, $Br(b \to c \to \ell)$ and $\langle X_b \rangle$ is calculated propagating the statistical errors given in Section 4.1 and taking into account their correlations. This leads to an error of $\pm 0.22 \times 10^{-3}$ on $Br(b \to X_u \ell \nu_\ell)$ mainly due to the uncertainty on $\langle X_b \rangle$. Neglecting correlations induces a negligible change in the error because of the very small sensitivity of the result to $Br(b \to X_c \ell \nu_\ell)$ and $Br(b \to c \to \ell)$ introduced by the normalization procedure, showing that the result is not sensitive to the knowledge of the statistical correlations.

The systematic errors induced by the modelling of $b \to c$ transitions have been evaluated varying the parameters of the model. Since the lepton p and $p_\perp$ spectra are very precisely measured [22], a variation of the parameters of the model produces also

relevant changes in $Br(b \to X_c \ell \nu_\ell)$, $Br(b \to c \to \ell)$ and $\langle X_b \rangle$ (see Table 4). These changes

Table 4: Contributions to the systematic uncertainty on $Br(b \to X_c \ell \nu_\ell)$ and $Br(b \to c \to \ell)$ (in %) and on $\langle X_b \rangle$ taken from Ref. [22].

| Source | Variation | $\Delta Br(b \to X_c \ell \nu_\ell)$ | $\Delta Br(b \to c \to \ell)$ | $\Delta \langle X_b \rangle$ |
|---|---|---|---|---|
| $b \to \ell$ modelling | 28% of $D^{**}$ | $^{+0.22}_{-0.12}$ | $^{-0.40}_{+0.32}$ | $^{+0.0072}_{-0.0127}$ |
| | 8% of $D^{**}$ | $^{-0.04}_{+0.04}$ | $^{+0.06}_{-0.06}$ | $^{+0.0008}_{-0.0008}$ |
| $B \to D$ modelling | (see Ref. [14]) | $^{+0.09}_{-0.12}$ | $^{+0.10}_{-0.15}$ | $^{-0.0018}_{+0.0023}$ |
| $c \to \ell$ model. | (see Ref. [14]) | | | |
| Electron ID efficiency | +2% | −0.12 | −0.13 | − |
| Photon conversions | +10% | +0.02 | −0.08 | −0.0004 |
| Electron background | +10% | − | −0.02 | −0.0001 |
| Muon ID efficiency | +2% | −0.11 | −0.07 | −0.0001 |
| Decaying hadrons | +10% | −0.11 | −0.07 | −0.0002 |
| Punch-through | +20% | +0.01 | −0.16 | −0.0001 |
| Punch + decays shape | | +0.08 | −0.03 | −0.0015 |
| $Br(b \to \psi \to \ell)$ | +14% | −0.02 | +0.01 | −0.0001 |
| $Br(b \to \tau \to \ell)$ | +18% | −0.04 | −0.06 | +0.0005 |
| $Br(b \to W \to \ell)$ | +50% | +0.01 | −0.14 | −0.0001 |

have been taken into account when evaluating the variations of $Br(b \to X_u \ell \nu_\ell)$.

As shown by Fig. 7, the shape of the $NN_{bu}$ distribution for b decays into $D^{**}$ is different from the shapes for the decays into D and $D^*$. Changing the fraction of $D^{**} + D^* \pi$ by $(18 \pm 10)\%$ according to the predictions of the ACCMM and ISGW2 models and taking into account the correlations with $Br(b \to X_c \ell \nu_\ell)$, $Br(b \to c \to \ell)$, and $\langle X_b \rangle$ results in a variation of $Br(b \to X_u \ell \nu_\ell)$ of $^{+0.06}_{-0.16} \times 10^{-3}$. If the correlations were ignored, the variation would be larger by a factor of eight.

To verify that this cancellation caused by the experimentally known lepton spectrum is not accidental, the relative impacts of $Br(b \to X_c \ell \nu_\ell)$, $Br(b \to c \to \ell)$, and $\langle X_b \rangle$ and of their correlations on $Br(b \to X_u \ell \nu_\ell)$ were modified. To do so, the fit was repeated, including or not the first two bins of the $NN_{bu}$ distribution. As shown in Table 5, the central value of $Br(b \to X_u \ell \nu_\ell)$ does not change significantly in the three fits while, for instance, the impact of $Br(b \to X_c \ell \nu_\ell)$ decreases by a factor of five when the first bin is removed and by a factor of ten when the first two bins are removed.

Table 5: Effect of the normalization procedure on the $Br(b \to X_u \ell \nu_\ell)$ value and on the systematic error due to the change of the fraction of $D^{**} + D^* \pi$ from 18% to 28% (see the text for more details). All the numbers of this table are given in units of $10^{-3}$.

| Cut on $NN_{bu}$ | Fitted $Br(b \to X_u \ell \nu_\ell)$ | $\Delta Br(b \to X_u \ell \nu_\ell)$ without correlations | $\Delta Br(b \to X_u \ell \nu_\ell)$ with correlations |
|---|---|---|---|
| 0.0 | $1.69 \pm 0.50$ | +1.04 | +0.14 |
| 0.1 | $1.73 \pm 0.55$ | +0.61 | +0.06 |
| 0.2 | $1.71 \pm 0.60$ | +0.45 | −0.10 |

To verify that this cancellation is not accidentally due to the specific shape of the $b \to c$ background, its shape was modified changing other parameters of the model (i.e., the topological branching ratios of the D mesons) and the procedure to evaluate the systematic error induced by the $D^{**} + (D^*\pi)$ fraction was repeated. No significant change in the error was observed.

The ratio $D^{**}/(D^*\pi)_{\rm nonres}$ has been varied by $1.0 \pm 0.5$ [30] for a given lepton momentum spectrum, to take into account the fact that the invariant mass distribution is broader in the nonresonant case [31]. This results in a change of $Br(b \to X_u \ell \nu_\ell)$ of $\pm 0.04 \times 10^{-3}$.

The rate of four body decay, $\Lambda_b \to \Lambda_c X \ell \nu_\ell$, in the semileptonic decays of the $\Lambda_b$ is varied by $(20 \pm 20)\%$ [32].

The modelling of the $b \to c \to \ell$ transitions is studied by fitting the DELCO and MARKIII data with the ACCMM model for the $c \to \ell$ part, and by using the measured $B \to D$ spectrum from CLEO for the $b \to c$ part [14].

The impact of prompt leptons coming from other b decays ($b \to \tau \to \ell$, $b \to \psi \to \ell$ and $b \to \bar{c} \to \ell$) is negligible.

The error associated to the lepton identification algorithm [9] has been propagated to $Br(b \to X_u \ell \nu_\ell)$ using the corrections shown in Table 4. The resulting variations of $Br(b \to X_u \ell \nu_\ell)$ are small.

### 7.1.4 Decay properties of the c hadrons

Since the analysis is sensitive to the charged multiplicity, the neural network output for background transitions has different shapes for different numbers of selected charged particles, hence the analysis is sensitive to the uncertainties on the topological branching ratios $B_i$. The associated systematic uncertainty is estimated as in Ref. [27]. The systematic uncertainties associated to the different channels are given in Table 6. In

Table 6: A breakdown of the uncertainties on $Br(b \to X_u \ell \nu_\ell)$ due to the topological branching ratios of D mesons.

| Source | Variation | $\Delta Br(b \to X_u \ell \nu_\ell)$ $(10^{-3})$ |
|---|---|---|
| $D^+ \to 1$ prong | $0.384 \pm 0.023$ | $\mp 0.13$ |
| $D^+ \to 5$ prongs | $0.075 \pm 0.015$ | $\pm 0.07$ |
| $D^0 \to 0$ prong | $0.054 \pm 0.011$ | $\mp 0.16$ |
| $D^0 \to 4$ prongs | $0.293 \pm 0.023$ | $\pm 0.09$ |
| $D^0 \to 6$ prongs | $0.019 \pm 0.009$ | $\pm 0.02$ |
| $D_s \to 1$ prong | $0.37 \pm 0.10$ | $\mp 0.18$ |
| $D_s \to 5$ prongs | $0.21 \pm 0.11$ | $\mp 0.05$ |

the MARKIII analysis [15], the systematic uncertainties on the topological branching ratios of the $D^+$ and $D^0$ mesons represent about 50% of their total error, of which half due to their charged particle track selection. This last contribution is then treated as fully correlated among the different channels, and added linearly to compute the systematic effect on $Br(b \to X_u \ell \nu_\ell)$. The errors on the topological branching ratios of the $D_s^+$ mesons are dominated by the statistical uncertainties and are therefore added in quadrature. Since no measurement is available for the topological final states of the $\Lambda_c$, it is assumed

that $\Delta B_1 = \pm 0.10$ and $\Delta B_5 = \pm 0.11$, the central values being given by the Monte Carlo. This leads to an error of $\pm 0.11 \times 10^{-3}$ on $Br(b \to X_u \ell \nu_\ell)$.

The systematic uncertainty due to the knowledge of the neutral multiplicity was evaluated varying the number of $\pi^0$ per D meson decay (for the $D^+$, the $D^0$ and the $D_s$) according to the results of Ref. [15].

The sensitivity of the neural network output to resonant decay modes of the D mesons like $D \to K^0_S X$, $D \to K^0_L X$, $D \to \rho X$, $D^+ \to \rho^+ K^0$ was studied for the $D^+$, $D^0$ and $D_s$ mesons by varying the associated branching ratios within their measured errors. The effect on $Br(b \to X_u \ell \nu_\ell)$ is negligible since none of the input variables has explicit resonance selection criteria in its definition. The most important effect comes from the final states containing an energetic neutral hadron (not considered in the reconstruction of the hadronic system X) as they are in turn characterized by low multiplicities and small reconstructed invariant masses. For the $\Lambda_c$, the decay modes $\Lambda_c \to \Lambda^0 X$, $\Lambda_c \to \Sigma^+ X$, $\Lambda_c \to pX$ and $\Lambda_c \to nX$ were considered. The largest effect comes from the final states with a neutron (Fig. 11).

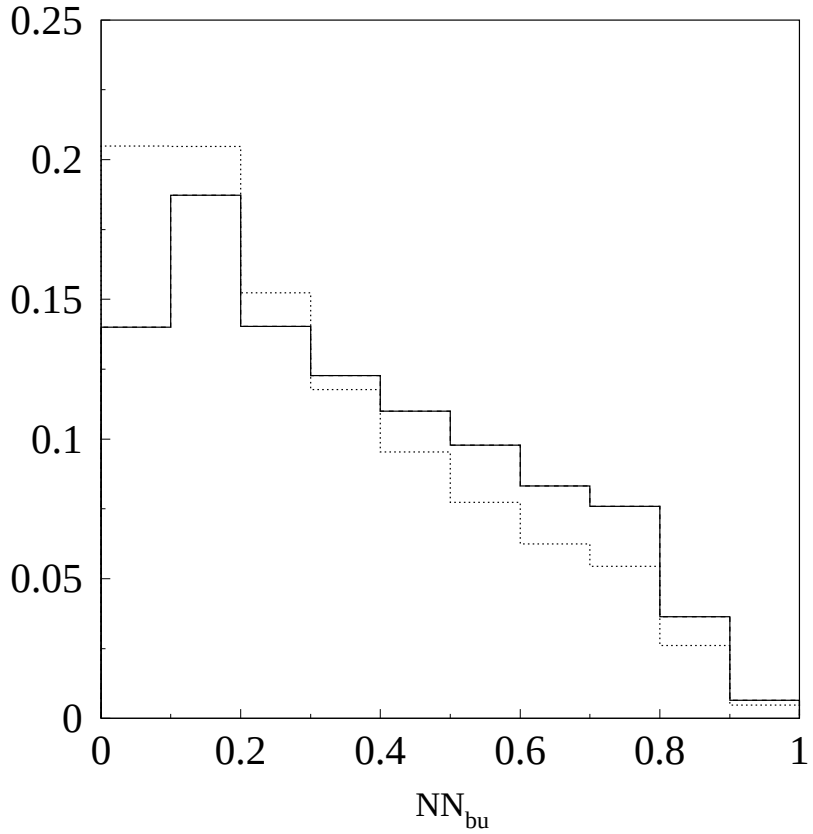


Figure 11: Output of $NN_{bu}$ for simulated $\Lambda_c$ decays with (solid line) and without (dotted line) a neutron in the final state. The two contributions are normalized to the same area.

Since the $D^+$ and $D^0$ are associated to different topological channels, their associated neural network outputs have different shapes, hence the analysis is sensitive to the ratio of their production rates in b hadron decays ($D^0/D^+ = 2.59 \pm 0.52$ [16]).

## 7.2 The $b \to X_u \ell \nu_\ell$ modelling

As stated earlier, the neural network variables were chosen to minimize the model dependence of the measurement. Figure 12 shows the distortions of the lepton momentum and of the hadronic mass spectra with the cut on $NN_{bu}$. It can be seen that even if $NN_{bu}$ is correlated with the two distributions, the cut $NN_{bu} > 0.6$, which is used in the analysis, selects events with $E_\ell^\star$ as low as 1 GeV and with any hadronic mass, illustrating that the method has reduced model dependence. The residual model dependence of the measurement is evaluated by varying the parameters of the hybrid model used for the simulation as follows.

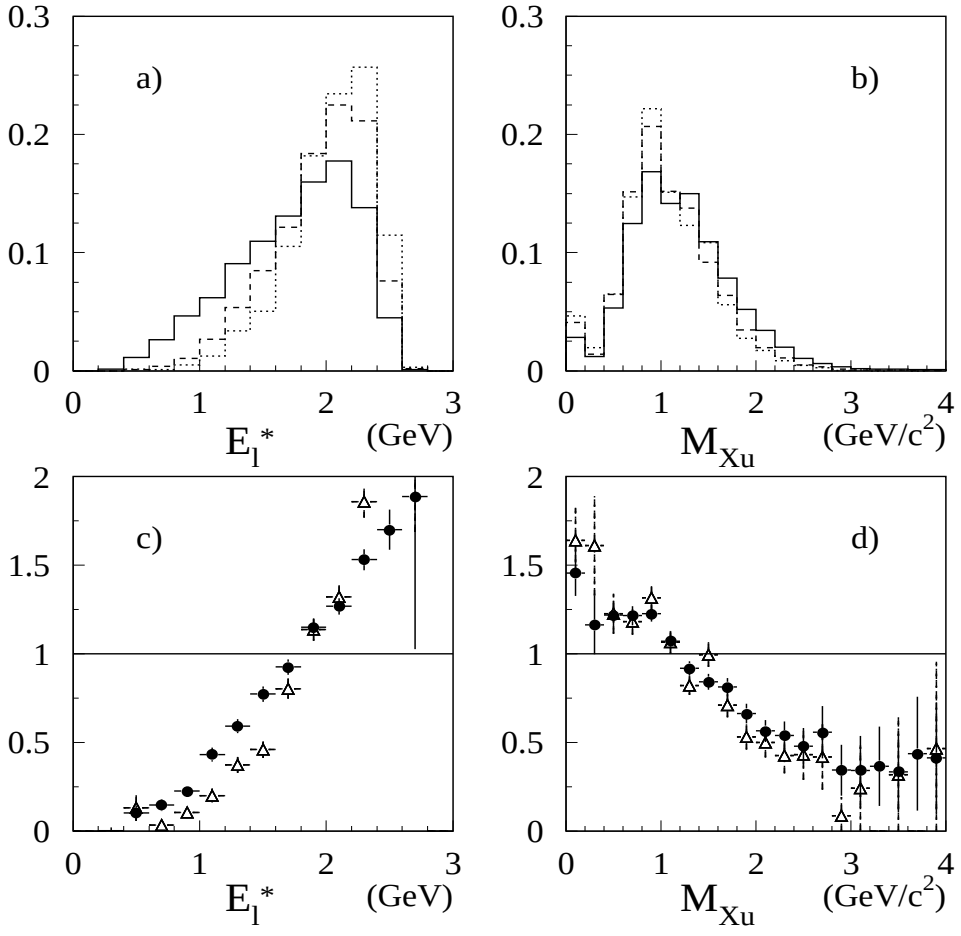


Figure 12: a) Lepton energy distribution in the b hadron centre-of-mass frame, and b) invariant mass of the hadronic system obtained in $b \to u \ell \nu_\ell$ transitions with a cut on $NN_{bu}$ at 0.0 (solid lines), 0.6 (dashed lines) and 0.8 (dotted lines); c) (resp. d)) shows the ratio of histogram a) (resp. b)) with cut at 0.6 (points) and 0.8 (triangles) to the histogram with no cut.

The energy cutoff parameter $\Lambda$ is varied to produced either only nonresonant or only resonant final states. The respective changes in the branching ratio $\mathrm{Br}(\mathrm{b} \to \mathrm{X_u}\ell\nu_\ell)$ are $+0.06 \times 10^{-3}$ and $-0.10 \times 10^{-3}$, confirming a small sensitivity to the details of the $\mathrm{X_u}$ final state. Then, with a cutoff parameter at the nominal value of 1.6 GeV and using the DSU model for the inclusive part, the exclusive model is changed from ISGW2 to that implemented in JETSET 7.4 [13]. This changes the branching ratio by $-0.05 \times 10^{-3}$. Further, again with $\Lambda = 1.6$ GeV, the inclusive part is changed from DSU to ACCMM and the parton [33] models with the exclusive part fixed as ISGW2. This gives a change of $-0.18 \times 10^{-3}$ for ACCMM and $-0.08 \times 10^{-3}$ for the parton model. The systematic uncertainty on $\mathrm{Br}(\mathrm{b} \to \mathrm{X_u}\ell\nu_\ell)$ is then obtained by taking the largest variation between the ACCMM and the parton models. Changing the values of $\mu_\pi^2$ and $m_\mathrm{b}$ within their errors leads to negligible variations in $\mathrm{Br}(\mathrm{b} \to \mathrm{X_u}\ell\nu_\ell)$.

The lepton momentum, the hadronic invariant mass and the $q^2$ distributions obtained with these three models are shown in Fig. 13.

Since there are no theoretical predictions for the charmless semileptonic transitions of the $\Lambda_\mathrm{b}$, two extreme choices have been made for the hadronic final state $\mathrm{X_u}$: *(i)* exclusive $\Lambda_\mathrm{b} \to \mathrm{p}\ell\nu_\ell$ transitions, and *(ii)* multi-body decays $\Lambda_\mathrm{b} \to [(\mathrm{p\ or\ n}) + \mathrm{n}\pi]\ell\nu_\ell$. The full difference obtained on $\mathrm{Br}(\mathrm{b} \to \mathrm{X_u}\ell\nu_\ell)$ with the two options is taken as the systematic.

### 7.3 Summary

The various sources of systematic uncertainties and their respective contributions on $\mathrm{Br}(\mathrm{b} \to \mathrm{X_u}\ell\nu_\ell)$ are summarized in Table 3. The uncertainty due to the modelling of the $\mathrm{b} \to \mathrm{u}$ transitions is a factor of two smaller than the error due to the $\mathrm{b} \to \mathrm{c}$ transitions.

This leads to the final result:

$$\mathrm{Br}(\mathrm{b} \to \mathrm{X_u}\ell\nu_\ell) = (1.73 \pm 0.55_{\mathrm{stat}} \pm 0.51_{\mathrm{syst\ b\to c}} \pm 0.21_{\mathrm{syst\ b\to u}}) \times 10^{-3}.$$

## 8 Checks of the analysis

### 8.1 $\mathrm{b} \to \mathrm{X_c}\ell\nu_\ell$ transitions

Since this analysis is based on the comparison of the $\mathrm{NN_{bu}}$ distribution between data and Monte Carlo, it is interesting to see how data and Monte Carlo agree in the signal region when events with a reconstructed D meson are selected. The agreement observed gives confidence that the $\mathrm{b} \to \mathrm{X_c}\ell\nu_\ell$ transitions are well simulated in the region where an excess of events is to be observed (see Fig. 14). However, this test has a limited statistical accuracy in the signal region.

### 8.2 Fit region dependence

The determination of $\mathrm{Br}(\mathrm{b} \to \mathrm{X_u}\ell\nu_\ell)$ has been done separately in each of the last five bins of the $\mathrm{NN_{bu}}$ distribution and the results are summarized in Table 7. This table shows that all the measurements agree within the statistical errors and that the last four bins have the largest weights in the final result. Figure 15 shows the variation of $\mathrm{Br}(\mathrm{b} \to \mathrm{X_u}\ell\nu_\ell)$ as a function of the cut on $\mathrm{NN_{bu}}$. Its value is seen to be stable within the variation allowed by the uncorrelated statistical uncertainties.

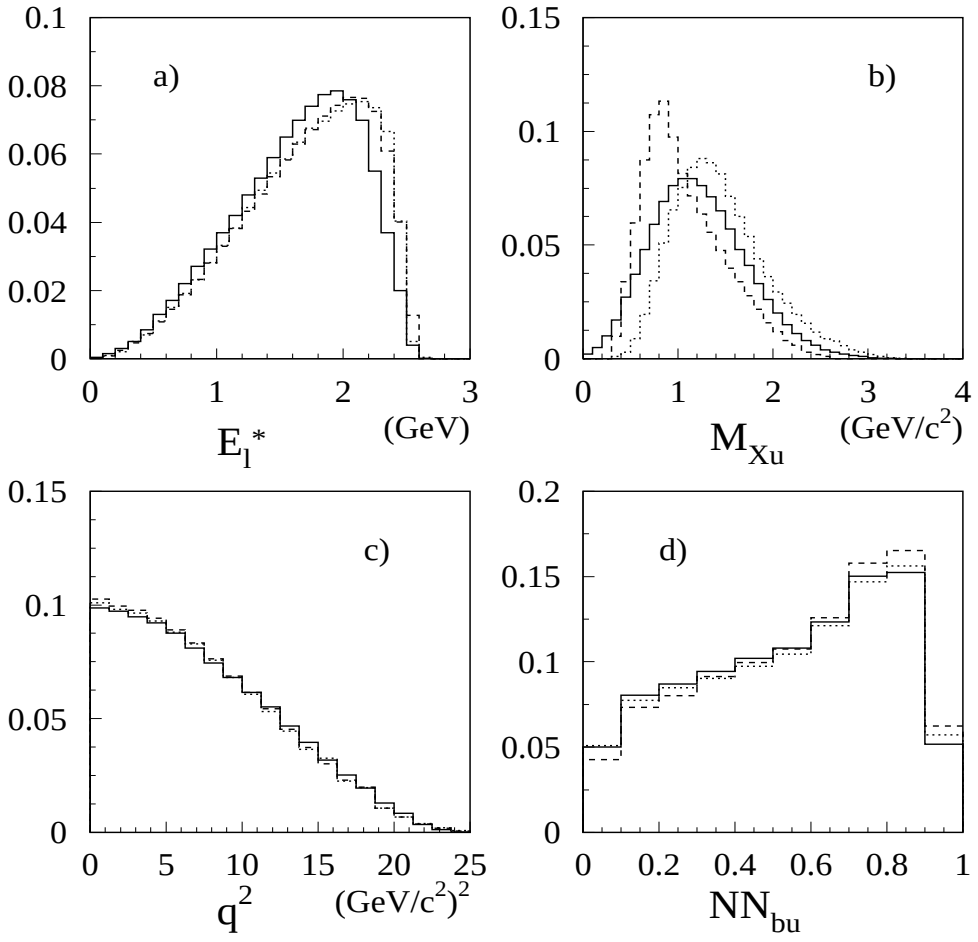


Figure 13: a) Lepton momentum, b) hadronic invariant mass, and c) $q^2$ of the virtual W for signal events as predicted by completely inclusive models: DSU model (solid lines), ACCMM model (dashed lines) and the parton model (dotted lines). d) shows the effect of the inclusive modelling on the $NN_{bu}$ output obtained with the hybrid model using $\Lambda = 1.6$ GeV and ISGW2 for the exclusive part.

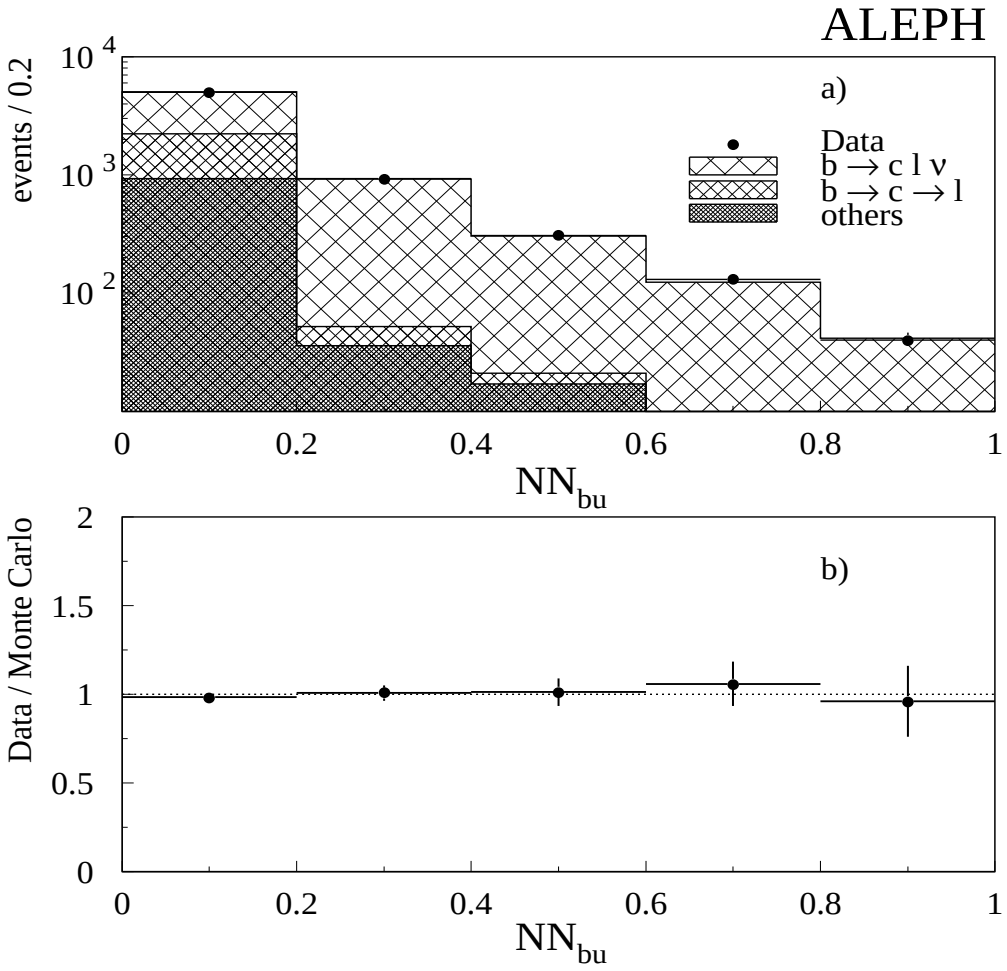


Figure 14: Neural network output $NN_{bu}$ for hemispheres with a lepton and a reconstructed D meson ($D^0 \to K^-\pi^+$, $D^0 \to K^-\pi^-\pi^+\pi^+$ and $D^+ \to K^-\pi^+\pi^+$). a) comparison between data (points) and Monte Carlo (histogram); b) ratio data/Monte Carlo as function of the neural network output $NN_{bu}$.

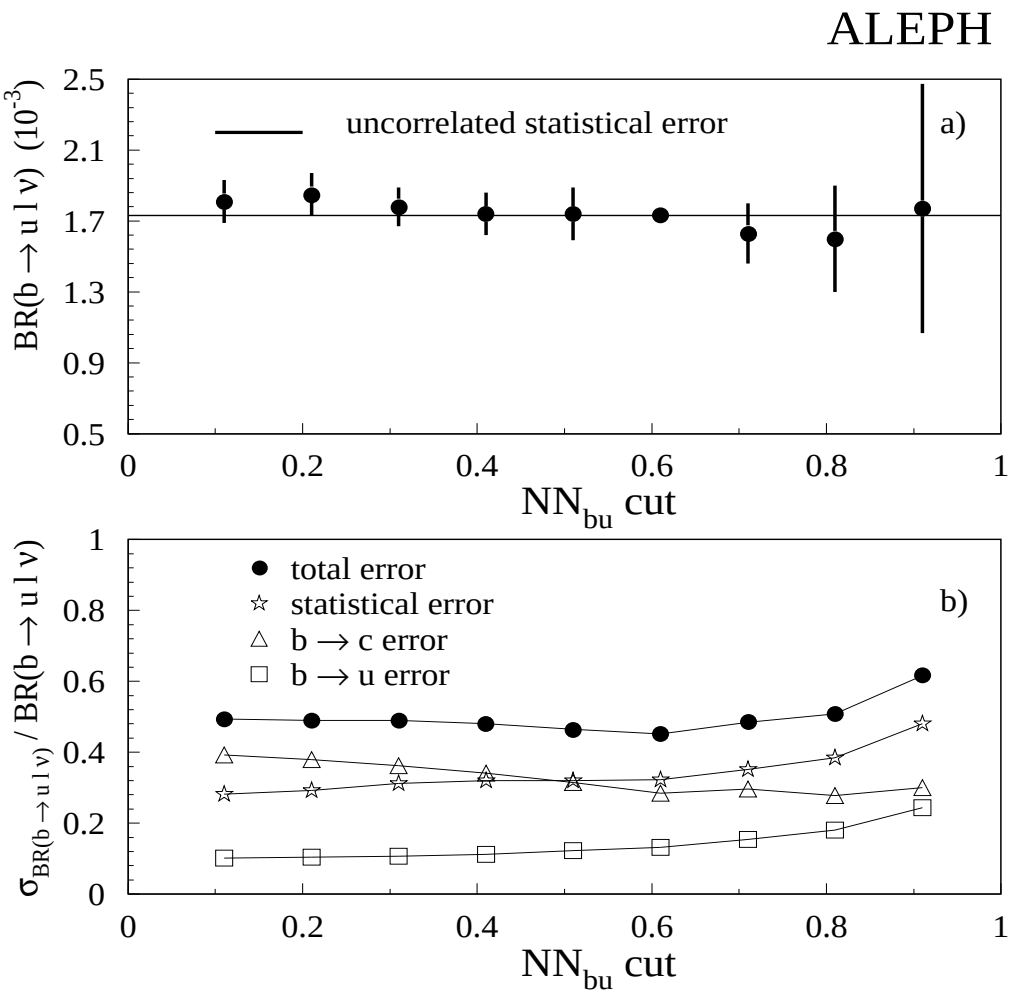


Figure 15: a) Values of the branching ratio Br($b \to X_u \ell \nu_\ell$) obtained for different cuts on $NN_{bu}$. The uncorrelated statistical errors are calculated with respect to the cut at 0.6; b) Relative errors obtained for the different cuts.

Table 7: Value of $Br(b \to X_u \ell \nu_\ell)$ obtained for each of the five last bins of $NN_{bu}$. The first error is statistical and the second is systematic.

| Fitted region | $Br(b \to X_u \ell \nu_\ell)$ $(10^{-3})$ |
|---|---|
| 0.5-0.6 | $2.2 \pm 3.7 \pm 2.0$ |
| 0.6-0.7 | $2.8 \pm 1.9 \pm 1.0$ |
| 0.7-0.8 | $1.8 \pm 1.5 \pm 0.9$ |
| 0.8-0.9 | $1.5 \pm 0.9 \pm 0.6$ |
| 0.9-1.0 | $1.8 \pm 0.9 \pm 0.6$ |

## 8.3 Detector effects

To quantify the effect of the detector resolution, the analysis has been repeated by replacing the real data events by Monte Carlo events with particle momenta computed at the generator level. This change is expected to have an unrealistically large effect on $Br(b \to X_u \ell \nu_\ell)$ since, for example, all photons from $\pi^0$ decays are separated at this level, thus leading to neutral multiplicities very different from the reconstructed ones, used in the neural network training. However, the fitted $Br(b \to X_u \ell \nu_\ell)$ value is decreased by 50% compared to the value used as input in the simulation, indicating that the detector effects related to subtle inaccuracies in the simulation can only have a minor influence on the final result.

The effect of the resolution on the neutrino energy and polar angle have been checked by reweighting the events according to their generated distributions so that they reproduce the generated ones. In both cases, the variation of $Br(b \to X_u \ell \nu_\ell)$ is negligible.

## 8.4 Change of the input variables

The standard analysis was changed in the following way: the BTCONE algorithm was used instead of $NN_c$ and $NN_\gamma$ to select the particles which enter the definition of the input variables; 15 of the 20 variables were replaced by 15 new variables; the new set of input variables was computed in the laboratory frame and was used as input of a new neural network called $NN'_{bu}$. This introduces a sensitivity of the analysis to b fragmentation which allows for a two parameter fit of $Br(b \to X_u \ell \nu_\ell)$ and of $\langle X_b \rangle$ as a consistency check. The definition of the input variables is given in the Appendix. As for the standard analysis, the comparison between the data and the simulation without $b \to u$ transitions shows an excess of events in the signal region (see Fig. 16). The one parameter fit gives $Br(b \to X_u \ell \nu_\ell) = (1.6 \pm 0.6_{stat}) \times 10^{-3}$, and the two parameter fit leads to $Br(b \to X_u \ell \nu_\ell) = (1.4 \pm 0.8_{stat}) \times 10^{-3}$; $\langle X_b \rangle = 0.711 \pm 0.005_{stat}$. The results are in agreement with the standard analysis.

## 8.5 Neutral hadron production

Since neutral hadrons are not considered when reconstructing the b hadron, a bad simulation of the $b \to X_c \ell \nu_\ell$ final states involving energetic neutral hadrons would alter the background $NN_{bu}$ distribution at high values (low reconstructed mass, low multiplicity) and therefore modify in either direction the measured $b \to u$ transition rate in the data.

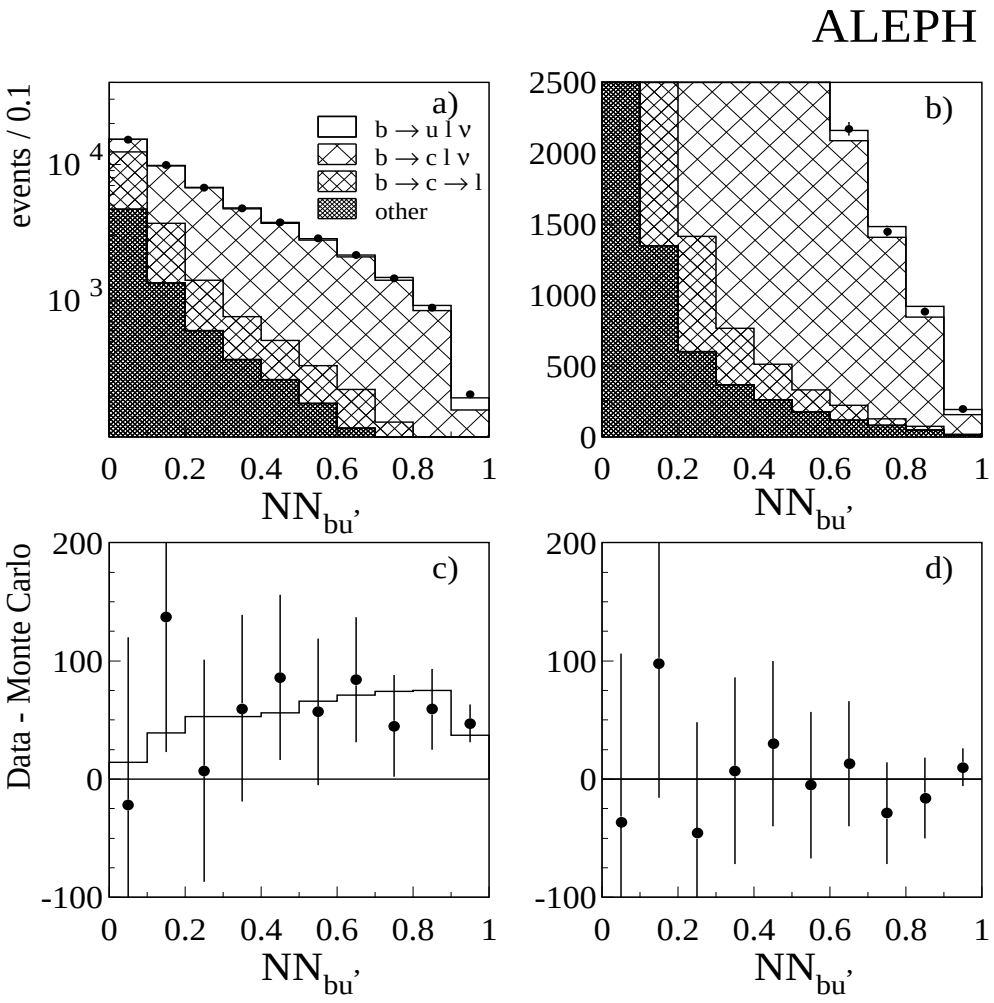


Figure 16: Neural network output $NN'_{bu}$: a) and b) comparison between data (points) and Monte Carlo (histogram), c) difference between data and Monte Carlo with no $b \to u$ transitions (points) compared to the $b \to u$ contribution (histogram), and d) difference between data and Monte Carlo with the fitted value of $b \to u$.

Figure 17 shows the neutral hadronic energy reconstructed in a 30° cone around the lepton for different cuts on $NN_{bu}$. Good agreement is observed between data and simulation for all the cuts. In particular, no excess/deficit appears in the data when the cut on $NN_{bu}$ is tightened. The neutral hadronic energy distribution is different for final states with and without $K^0_L$ (Fig. 18), providing the opportunity to measure the inclusive production rate of $K^0_L$ in D meson decays, as a consistency check. The results are summarized in Table 8. They are in agreement with each other and with the average value of $(24.5 \pm 4.4)\%$ measured by MARKIII [15].

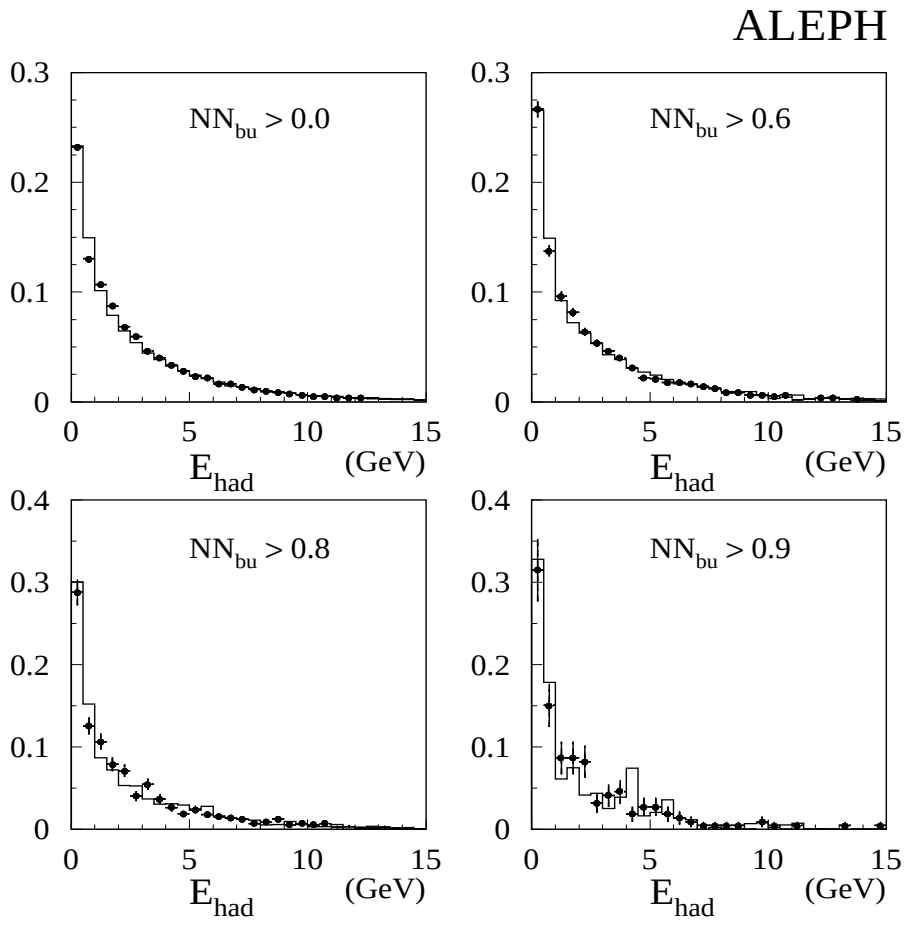


Figure 17: Neutral hadronic energy deposited in a 30° cone around the lepton. Comparison between data (points) and Monte Carlo (histogram) for several cuts on $NN_{bu}$.

## 8.6 Evidence for b → u signal in $M_B^{rec}$ distribution

The b → c events associated to high values of $NN_{bu}$ ($NN_{bu} > 0.9$) often contain a badly reconstructed hadronic system $X_c$ with unusually low multiplicity and mass. As a consequence, the invariant mass $M_B^{rec}$ of the $X_c \ell \nu_\ell$ system is not peaked at 5.4 GeV/$c^2$ but has a rather broad distribution, in contrast to well reconstructed b → u events (Fig. 19a). This gives the opportunity to search for evidence of b → u in this

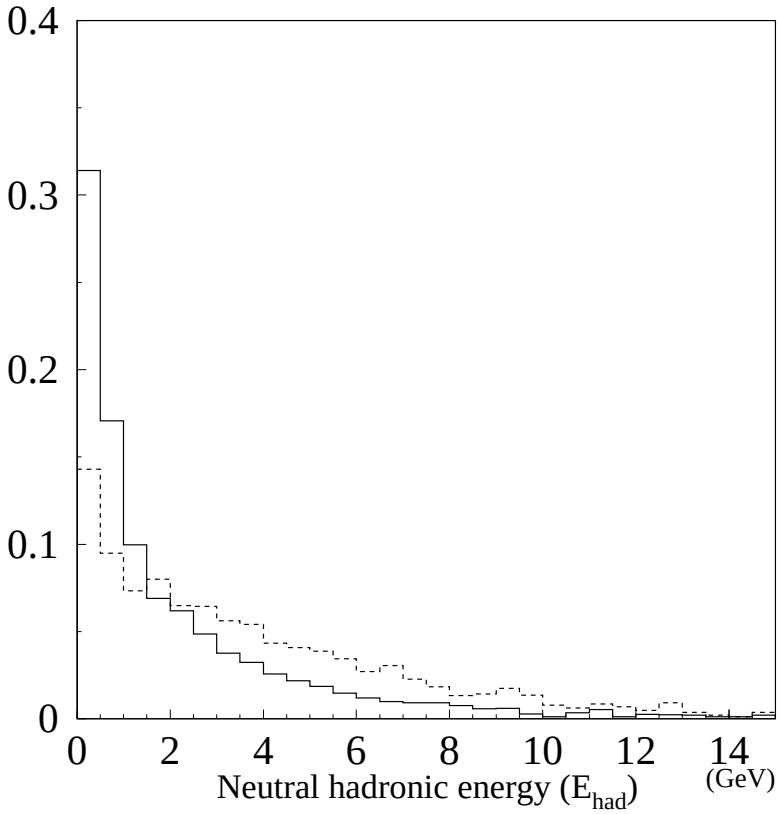


Figure 18: Simulated neutral hadronic energy deposited in a 30° cone around the lepton for events with (dashed histogram) and without (solid histogram) $K^0_L$. The two contributions are normalized to the same area.

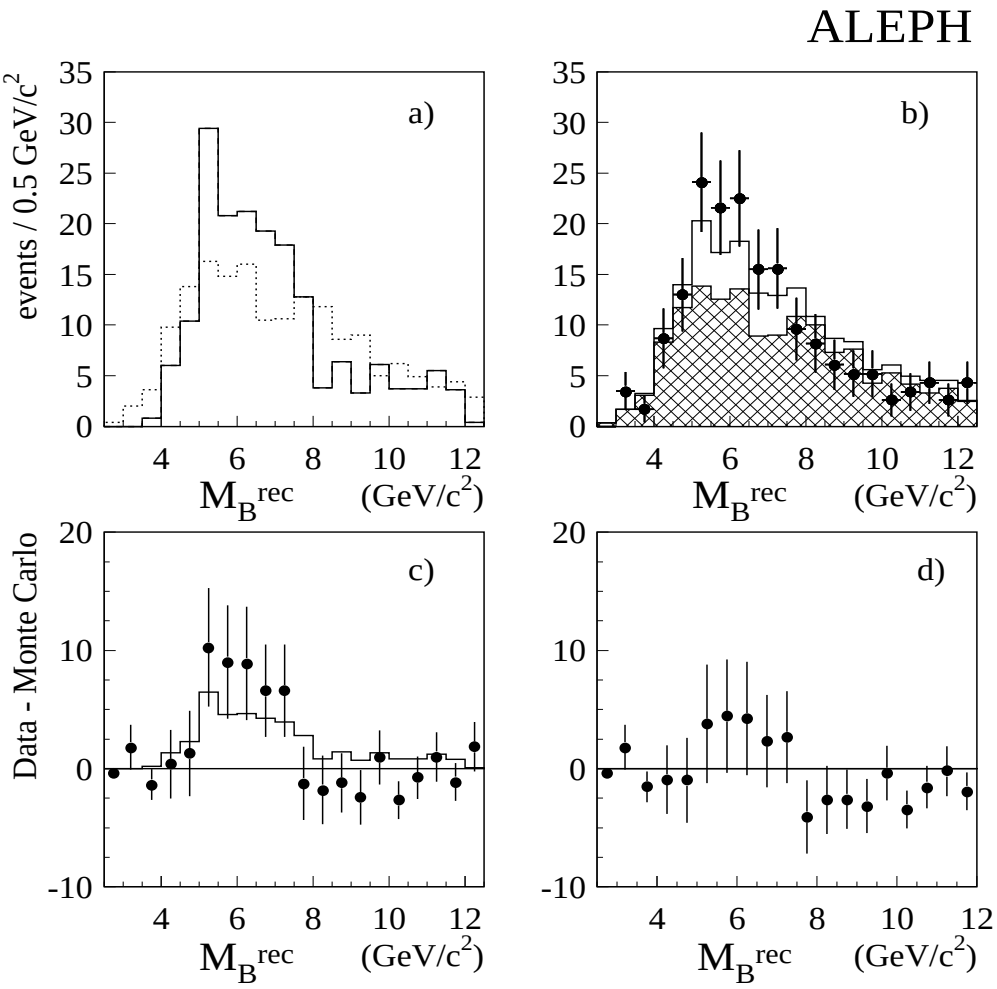


Figure 19: Invariant mass $M_B^{rec}$ of the reconstructed X$\ell\nu_\ell$ system in the region $NN_{bu} > 0.9$. a) Comparison between simulated b $\rightarrow$ u (solid histogram) and b $\rightarrow$ c (dotted histogram) transitions (the two distributions are normalized to the same area); b) comparison between data (points) and Monte Carlo. The hatched histogram is for b $\rightarrow$ c transitions and the open one describes the b $\rightarrow$ u contribution. c) Difference between data and Monte Carlo with no b $\rightarrow$ u transitions (points) compared to the b $\rightarrow$ u contribution (histogram), and d) difference between data and Monte Carlo with the fitted value of b $\rightarrow$ u.

Table 8: Average values, obtained for different cuts on $NN_{bu}$, of the neutral hadronic energy $E_{had}$ (in GeV) deposited in a 30° cone around the lepton, and fitted values of the inclusive production rate of $K^0_L$ in D meson decays. The errors are statistical only.

| Cut on $NN_{bu}$ | $\langle E_{had} \rangle_{data}$ | $\langle E_{had} \rangle_{MC}$ | $Br(D \to K^0_L X)$ (%) |
|---|---|---|---|
| 0.0 | $2.66 \pm 0.01$ | 2.69 | $24.2 \pm 1.0$ |
| 0.6 | $2.55 \pm 0.04$ | 2.56 | $24.7 \pm 2.0$ |
| 0.8 | $2.41 \pm 0.07$ | 2.36 | $24.0 \pm 4.4$ |
| 0.9 | $2.10 \pm 0.15$ | 2.10 | $17.9 \pm 9.0$ |

distribution. Good agreement is observed between data and Monte Carlo except in the region $4 < M_B^{rec} < 8$ GeV/c$^2$ where an excess of events is seen to be compatible with the measured signal $b \to X_u \ell \nu_\ell$ transitions. This exercise cannot be repeated with the hadronic invariant mass $M_X$ since, as mentioned above, the selection of events with $NN_{bu}$ larger than 0.9 biases the background towards low (badly reconstructed) $M_X$ (Fig. 20).

## 8.7 Evidence of b → u transitions in the vertexing

Since no vertexing information is used in the input variables, an independent signature of $b \to u$ transitions at high values of $NN_{bu}$ can be constructed. A common vertex between the lepton candidate and the charged hadronic system $X_{ch}$ is reconstructed and the corresponding $\chi^2$ calculated. To select only well defined secondary vertices, a cut at 0.2 on the $\chi^2$ probability is applied [34]. The efficiency of this cut is then determined for data and Monte Carlo events for different cuts on $NN_{bu}$. Because of the c hadron lifetime, this efficiency is expected to be smaller for $b \to c$ compared to $b \to u$ transitions (Fig. 21a). This effect becomes even more important at high values of $NN_{bu}$ because the $b \to c$ events which populate this region, *(i)* have small charged multiplicity, and *(ii)* are often not well reconstructed, as already discussed, thus giving a poor vertex fit (Fig. 21b). Figure 22 shows the ratio of these efficiencies between data and simulation with and without $b \to u$ transitions. No dependence on $NN_{bu}$ is seen if the data are compared to the simulation including $b \to u$ events, while this ratio increases with the cut on $NN_{bu}$ with pure $b \to c$ simulated events, indicating the presence of $b \to u$ transitions in the data at high $NN_{bu}$ values.

## 8.8 A few $b \to X_u \ell \nu_\ell$ candidate events

Finally, the 192 data events with $NN_{bu} > 0.9$ have been visually inspected to search for direct evidence of $b \to X_u \ell \nu_\ell$ transitions. A total of 35 events is expected to come from $b \to u$ transitions (as determined from the fitted value of the branching fraction), of which 3.8 from $X_u = \pi^-$ or $\rho^-$. Two such events were found and the $B^0 \to \rho^- e^+ \nu_e$ candidate event is shown in Fig 23.

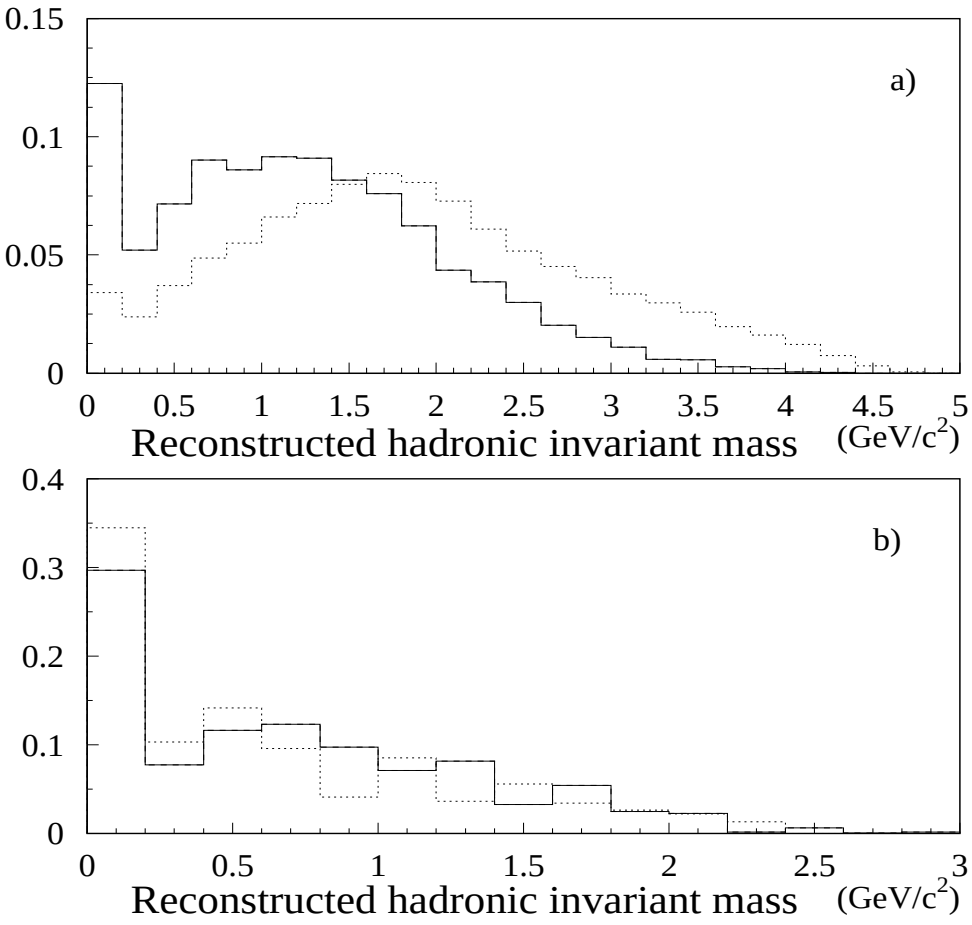


Figure 20: Comparison of the reconstructed hadronic invariant mass $M_X$ in simulated $b \to u$ (solid line) and $b \to c$ (dotted line) events, a) with no cut on $NN_{bu}$, b) for $NN_{bu} > 0.9$. The two distributions are normalized to the same area.

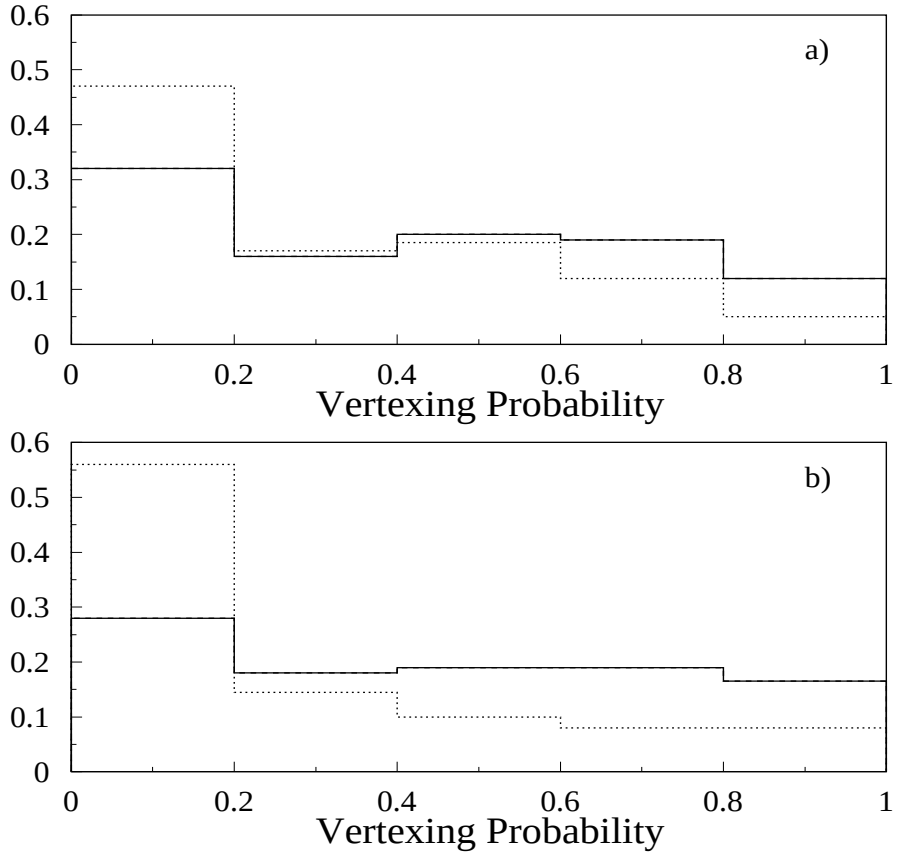


Figure 21: Probability of the lepton-$X_{\rm ch}$ vertex with: a) no cut on $\rm NN_{bu}$ and b) $\rm NN_{bu} > 0.8$. Comparison between simulated $\rm b \to X_c \ell \nu_\ell$ (dotted line) and $\rm b \to u$ (solid line) transitions.

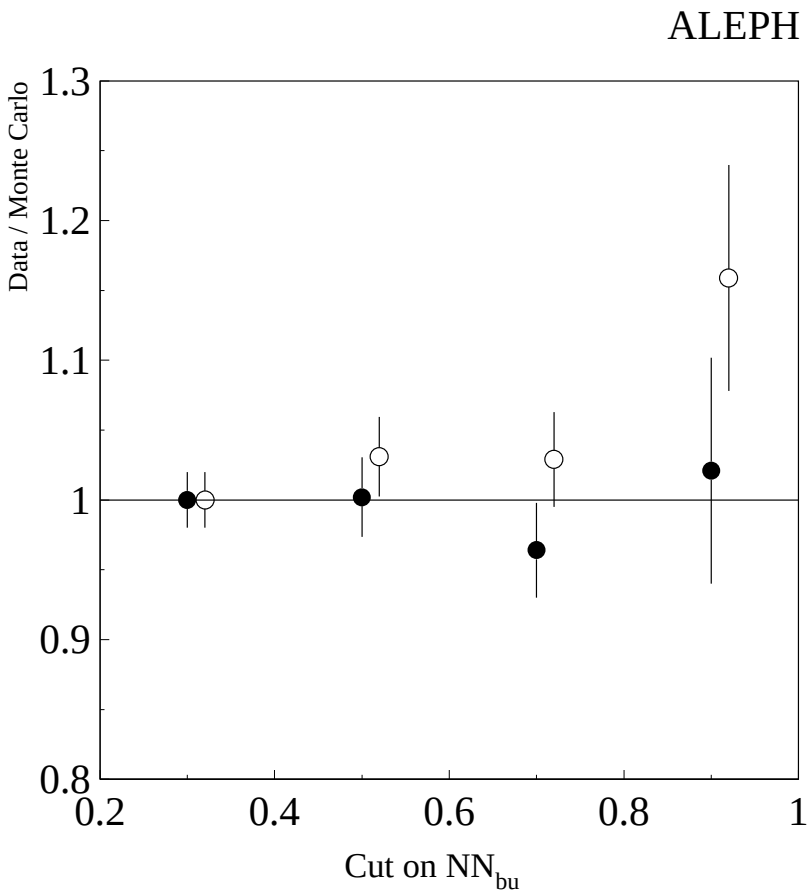


Figure 22: Ratio of vertexing efficiencies between data and Monte Carlo as a function of the cut applied on $NN_{bu}$, with (black circles) and without (open circles) b $\rightarrow$ u transitions in the simulation. The ratios are normalized to have a value equal to 1 for $NN_{bu} = 0.3$.

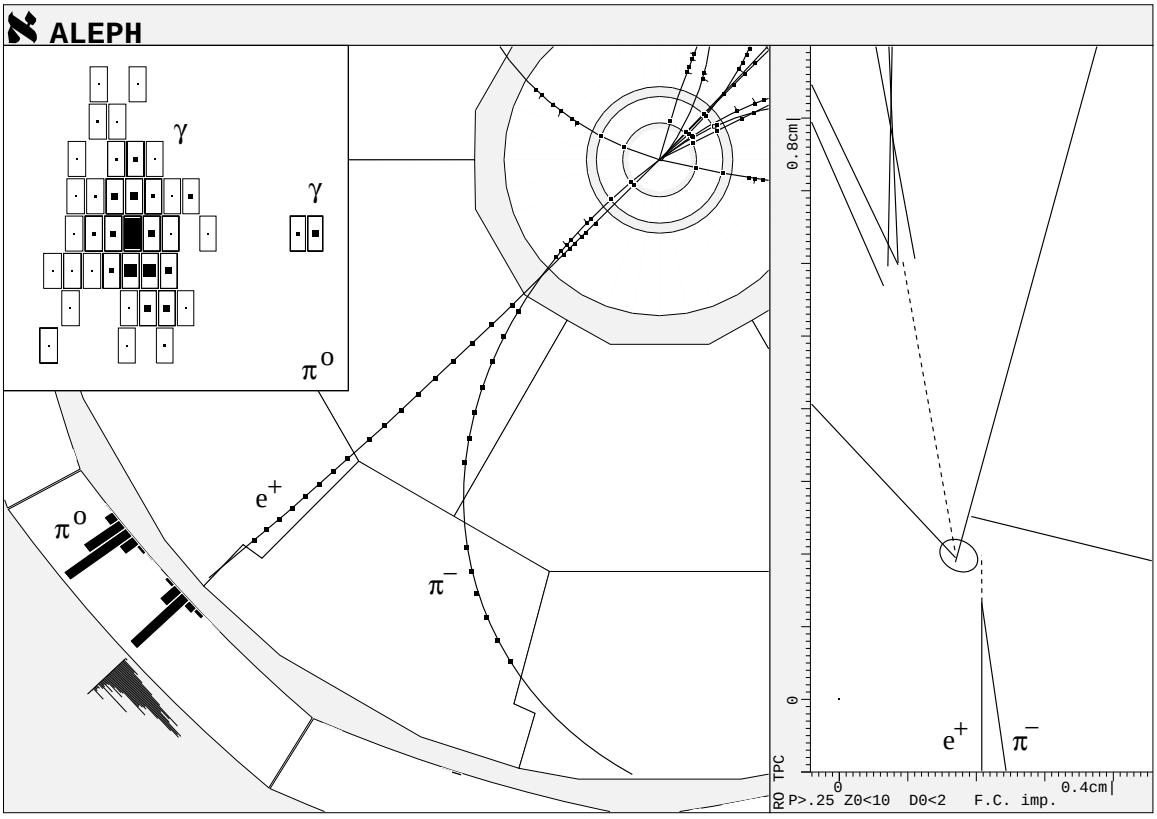


Figure 23: View of the scanned $B^0 \to \rho^- e^+ \nu_e$ event, with $\rho^- \to \pi^- \pi^0$ and $\pi^0 \to \gamma\gamma$. The right plot shows a close up $r\phi$ view of the interaction point with the $3\sigma$ ellipse corresponding to the primary vertex of the event and the detached vertex formed by the $e^+$ and the $\pi^-$ candidates, while the upper left insert shows the energy deposited in the electromagnetic calorimeter by the two photons coming from the $\pi^0$ decay.

# 9 Determination of $|V_{ub}|$

The value of $|V_{ub}|$ is determined from the measurement of the inclusive charmless semileptonic branching ratio of b hadrons by using the relation obtained in the framework of the Heavy Quark Expansion theory [36]:

$$|V_{ub}|^2 = 20.98 \frac{Br(b \to X_u \ell \nu_\ell)}{0.002} \frac{1.6 \text{ ps}}{\tau_B} (1 \pm 0.05_{pert} \pm 0.06_{m_b}) \times 10^{-6}$$

where $\tau_B$ is the average b hadron lifetime. With $\tau_B = (1.554 \pm 0.013)$ ps [35], $|V_{ub}|^2$ is determined to be

$$|V_{ub}|^2 = (18.68 \pm 5.94_{stat} \pm 5.94_{syst} \pm 1.45_{HQE}) \times 10^{-6},$$

where the last error comes from the uncertainties on $m_b$ and on higher-order perturbative corrections [36].

This measurement yields $|V_{ub}| = (4.16 \pm 1.02) \times 10^{-3}$ in agreement with the value $(3.3 \pm 0.8) \times 10^{-3}$ derived by CLEO using exclusive final states [2]. In contrast to the errors assigned to $|V_{ub}|^2$, those assigned to $|V_{ub}|$ are not Gaussian and ought to be used with care. For instance, the "two sigma" interval turns out to be asymmetric: $|V_{ub}| = (4.16^{+1.86}_{-2.80}) \times 10^{-3}$ at the 95% confidence level, instead of the $\pm 2.04 \times 10^{-3}$ that could be naively derived from the previous equation.

# 10 Conclusion

Using a tag based on the different kinematic properties of the final states $b \to X_u \ell \nu_\ell$ and $b \to X_c \ell \nu_\ell$, the inclusive charmless semileptonic branching ratio of b hadrons has been measured. The analysis of data collected between 1992 and 1995 leads to

$$Br(b \to X_u \ell \nu_\ell) = (1.73 \pm 0.55_{stat} \pm 0.55_{syst}) \times 10^{-3}.$$

The value of the CKM matrix element squared $|V_{ub}|^2$, extracted by using a model based on the Heavy Quark Expansion theory, is

$$|V_{ub}|^2 = (18.68 \pm 5.94_{stat} \pm 5.94_{syst} \pm 1.45_{HQE}) \times 10^{-6},$$

corresponding to $|V_{ub}| = (4.16 \pm 1.02) \times 10^{-3}$ with non-Gaussian errors.

# Acknowledgment

We are indebted to our colleagues of the accelerator divisions for the outstanding performance of the LEP accelerator. Thanks are also due to the many engineering and technical personnel at CERN and at the home institutes for their contributions toward the success of ALEPH. Those of us not from member states wish to thank CERN for its hospitality. We thank R. D. Dikeman and N. G. Uraltsev for their help in the simulation of charmless semileptonic B decays.

# Appendix

In the following, the input variables are ordered by decreasing discriminating power according to the value of their "inertial part" [37] (expressed in %). This fraction gives the amount of information carried by the associated variable.

## Input variables $G_{IP}$ used in $NN_\gamma$

- $G(1)_{38.4}$: The angle between the photon and the axis of the nucleated jet (see variable G(4) for definition of this axis).
- $G(2)_{34.8}$: The momentum of the photon.
- $G(3)_{23.4}$: The angle between the lepton and the photon.
- $G(4)_{3.4}$: The rapidity of the photon computed w.r.t. the axis of a nucleated jet defined as follows [38]: the lepton is chosen as initial axis. Then, the momenta of charged particles and photons of the lepton hemisphere are added to that of the lepton, taking first the particle which adds the least to the $\ell - X$ invariant mass. The addition is stopped when no particle can be added without increasing this invariant mass to a value greater than 5 GeV/$c^2$. Finally, the axis of this nucleated jet is defined by removing the momentum vector of the lepton.

## Input variables $C_{IP}$ used in $NN_c$

- $C(1)_{33.6}$: Same as G(3).
- $C(2)_{32.6}$: The track impact parameter divided by its error.
- $C(3)_{13.1}$: Same as G(2).
- $C(4)_{9.9}$: Same as G(4).
- $C(5)_{5.7}$: Same as G(1).
- $C(6)_{5.1}$: The track impact parameter.

## Input variables $V_{IP}$ used for $NN_{bu}$

The particles which enter the definition of the input variables $V_{IP}$ are selected in the lepton hemisphere by cutting on $NN_c$ and $NN_\gamma$ (see Section 3), and $p_\perp$ (resp. $p_{//}$) refers to the transverse (resp. longitudinal) momentum of a particle computed w.r.t. the lepton axis. Finally, the particle numbering 1, 2, 3, ... stands for the first, second, third, ... most energetic selected particle.

- $V(1)_{9.9}$: $[\sum_j(\sum_{i\leq j} p_\perp(i))(\sum_{i\leq j} p_{//}(i))]/[\sum_j p(j)]^2$ where the particles j are ordered by decreasing energy values.
- $V(2)_{8.0}$: Hadronic invariant mass of the charged particles.
- $V(3)_{8.0}$: Transverse momentum of the most energetic particle (lepton excluded).

- $V(4)_{7.3}$: Invariant mass $M_{1,2}$.
- $V(5)_{6.6}$: Charged particle multiplicity.
- $V(6)_{6.6}$: Fraction of the reconstructed energy carried by the lepton.
- $V(7)_{4.6}$: Sum of the rapidities of the charged particles w.r.t. the lepton axis.
- $V(8)_{4.5}$: Energy of the lepton in the reconstructed b hadron rest frame.
- $V(9)_{4.4}$: Rapidity of the most energetic particle computed w.r.t. the lepton axis.
- $V(10)_{4.3}$: Invariant mass $M_{1,3}$.
- $V(11)_{4.1}$: Transverse momentum of the second leading particle.
- $V(12)_{4.1}$: "Directed Sphericity" [39] for particles 1, 2 and 3.
- $V(13)_{4.1}$: Invariant mass $M_{1,4}$.
- $V(14)_{4.0}$: $\sum_j [p_\perp(j)]^2$.
- $V(15)_{3.9}$: Invariant mass $M_{2,3,4}$.
- $V(16)_{3.8}$: $\sum_j p_\perp(j) / \sum_j p(j)$.
- $V(17)_{3.5}$: Rapidity of the lepton w.r.t. the hemisphere axis.
- $V(18)_{3.4}$: Lepton transverse momentum computed w.r.t. the b boost axis.
- $V(19)_{3.2}$: Mass of the hadronic system X obtained with a nucleated jet algorithm.
- $V(20)_{2.5}$: Invariant mass $M_{1,3,4}$.

## Input variables $V'_{IP}$ used for $NN'_{bu}$

The particles which enter the definition of the input variables $V'_{IP}$ are selected in the lepton hemisphere with the BTCONE algorithm (see Section 3).

- $V'(1)_{11.6}$: Sum of the charged particle rapidities computed w.r.t. the lepton axis.
- $V'(2)_{7.0}$: Transverse momentum of the lepton w.r.t. its jet axis (lepton excluded).
- $V'(3)_{6.7}$: Rapidity of the lepton w.r.t. its jet axis.
- $V'(4)_{6.1}$: Transverse momentum of the most energetic particle (lepton excluded).
- $V'(5)_{5.2}$: $[\sum_j (\sum_{i \leq j} p_\perp(i))(\sum_{i \leq j} p_{//}(i))] / [\sum_j p(j)]^2$ where the particles j are ordered by decreasing energy values.
- $V'(6)_{5.1}$: $|\sum_j \vec{p}(j)|$.
- $V'(7)_{5.0}$: Invariant mass $M_{1,2,3}$.
- $V'(8)_{4.8}$: $[E_{lepton} + \sum_j E(j)] / E_{beam}$.

- $V'(9)_{4.8}$: Invariant mass $M_{1,2,4}$.
- $V'(10)_{4.6}$: "Directed Sphericity" of particles 1, 2 and 4.
- $V'(11)_{4.4}$: Transverse momentum of the second leading particle.
- $V'(12)_{4.4}$: $|\sum_j \vec{p}(j)|$ where j runs over all the selected charged particles.
- $V'(13)_{4.2}$: $|\vec{p}_{\rm lepton} + \sum_j \vec{p}(j)|$.
- $V'(14)_{4.1}$: Lepton-neutrino invariant mass.
- $V'(15)_{3.9}$: "Directed Sphericity" of particles 1, 2 and 3.
- $V'(16)_{3.9}$: Fraction of energy carried by the lepton.
- $V'(17)_{3.8}$: $\sum_j [p_\perp(j)]^2$.
- $V'(18)_{3.5}$: "Directed Sphericity" of the particles 1, 2, 3 and 4.
- $V'(19)_{3.5}$: Invariant mass of the lepton and charged particles.
- $V'(20)_{3.4}$: $|\vec{p}_{\rm lepton} + \sum_j \vec{p}(j)|$ where j runs over all the selected charged particles.

# References


[1] ARGUS Collaboration, *Observation of semileptonic charmless B meson decays*, Phys. Lett. **B234** (1990) 409; ARGUS Collaboration, *Reconstruction of semileptonic $b \to u$ decays*, Phys. Lett. **B255** (1991) 297.
CLEO Collaboration, *Observation of the B-Meson Semileptonic Decays to Noncharmed Final States*, Phys. Rev. Lett. **64** (1990) 16; CLEO Collaboration, *Measurement of Charmless Semileptonic Decays of B mesons*, Phys. Rev. Lett. **71** (1993) 4111.

[2] CLEO Collaboration, *First Measurement of $B \to \pi\ell\nu$ and $B \to \rho(\omega)\ell\nu$ Branching Fractions*, Phys. Rev. Lett. **77** (1996) 5000.

[3] R. D. Dikeman and N. G. Uraltsev, TPI-MINN-97/06-T, hep-ph/9703437; I. Bigi, R. D. Dikeman and N. G. Uraltsev, hep-ph/9706520.

[4] V. Barger *et al.*, Phys. Lett. **B251** (1990) 629; J. Dai, Phys. Lett. **B333** (1994) 212; A. Falk, *Extraction of $V_{ub}$ from the hadronic invariant mass spectrum in semileptonic B decays*, talk given at the EPS-HEP97, Jerusalem, August 1997.

[5] C. Ramirez, J. F. Donoghue and G. Burdman, Phys. Rev. **D41** (1990) 1496.

[6] ALEPH Collaboration, *ALEPH: a detector for electron-positron annihilations at LEP*, Nucl. Inst. and Meth. **A294** (1990) 121.

[7] ALEPH Collaboration, *Performance of the ALEPH detector at LEP*, Nucl. Inst. and Meth. **A360** (1995) 481.

[8] ALEPH Collaboration, *A precise measurement of* $\Gamma_{Z\to b\bar{b}}/\Gamma_{Z\to hadrons}$, Phys. Lett. **B313** (1993) 535.

[9] ALEPH Collaboration, *Heavy flavour production and decay with prompt leptons in the ALEPH detector*, Z. Phys. **C62** (1994) 179.

[10] ALEPH Collaboration, *Improved measurements of electroweak parameters from Z decays into fermion pairs*, Z. Phys. **C53** (1992) 1.

[11] ALEPH Collaboration, *Measurement of the effective b quark fragmentation function at the Z resonance*, Phys. Lett. **B357** (1995) 699.

[12] OPAL Collaboration, *QCD studies using a cone-based jet finding algorithm for* $e^+e^-$ *collisions at LEP*, Z. Phys. **C63** (1994) 197.

[13] T. Sjöstrand, Comp. Phys. Comm., **82** (1994) 74.

[14] ALEPH, DELPHI, L3 and OPAL Collaboration, *Combining heavy flavor electroweak measurements at LEP*, Nucl. Inst. and Meth. **A378** (1996) 101.

[15] MARKIII Collaboration, *Measurement of the inclusive decay properties of charmed mesons*, Phys. Lett. **B263** (1991) 135.

[16] Particle Data Group, *Review of Particle Physics*, Phys. Rev. **D54** (1996) 1.

[17] G. Altarelli *et al.*, Nucl. Phys. **B208** (1982) 365; G. Altarelli and S. Petrarca, Phys. Lett. **B261** (1991) 303.

[18] CLEO Collaboration, *Measurement of semileptonic branching fractions of B mesons at the* $\Upsilon(4S)$ *resonance*, Phys. Rev. **D45** (1992) 2212.

[19] DELCO Collaboration, *Semileptonic Decays on the D meson*, Phys. Rev. Lett. **43** (1979) 1073.

[20] MARKIII Collaboration, *Direct Measurement of charmed* $D^+$ *and* $D^0$ *Semileptonic Branching Ratios*, Phys. Rev. Lett. **54** (1985) 1976.

[21] CLEO Collaboration, *Inclusive and exclusive decays of B mesons to final states including charm and charmonium mesons*, Phys. Rev. **D45** (1992) 21.

[22] P. Perret, talk given at the EPS-HEP95, Brussel, July 1995;
S. Monteil, Ph-D Thesis, *Production et désintégrations semileptoniques des quarks lourds au LEP avec le détecteur ALEPH*, Clermont-Ferrand, PCCFT-9602.

[23] D. Scora and N. Isgur, Phys. Rev. **D52** (1995) 2783.

[24] R. D. Dikeman, M. Shifman and N. G. Uraltsev, Int. Jour. Mod. Phys. **A11** (1996) 571.

[25] M. B. Voloshin, Int. Jour. Mod. Phys. **A10** (1995) 2865.

[26] M. Neubert, *B Decays and CP Violation*, CERN-TH/96-55, April 1996.

[27] ALEPH Collaboration, *A measurement of $R_b$ using a lifetime-mass tag*, Phys. Lett. **B401** (1997) 150.

[28] L. Chaussard, *B hadron production and inclusive b decays at LEP*, talk given at the EPS-HEP97, Jerusalem, August 1997.

[29] ALEPH Collaboration, *Measurement of the $\Lambda_b$ polarization*, Phys. Lett. **B365** (1996) 437.

[30] ALEPH Collaboration, *Production of orbitally excited charm mesons in semileptonic B decays*, Z. Phys. **C73** (1997) 601.

[31] C. S. Kim *et al.*, Nucl. Phys. **B** (Proc. Suppl.) **37A** (1984) 69.

[32] ALEPH Collaboration, *Measurements of the b baryon lifetime*, Phys. Lett. **B357** (1995) 685.

[33] A. Bareiss and E. A. Paschos, Nucl. Phys. **B327** (1989) 353; C. H. Jin, W. F. Palmer and E. A. Paschos, Phys. Lett. **B329** (1994) 384; K. Y. Lee and J. K. Kim, Phys. Lett. **B379** (1996) 202.

[34] ALEPH Collaboration, *An investigation of $B_d^0$ and $B_s^0$ oscillations*, Phys. Lett. **B322** (1994) 441.

[35] F. Muheim, *A review of b hadron lifetimes*, talk given at the EPS-HEP97, Jerusalem, August 1997.

[36] N. G. Uraltsev, Int. Jour. Mod. Phys. **A11** (1996) 515; I. Bigi, M. Shifman and N. G. Uraltsev, hep-ph/9703290.

[37] C. Guicheney, Preprint Clermont-Fd, PCCF-9401 (1994).

[38] ALEPH Collaboration, *Measurements of mean lifetime and branching fractions of b hadrons decaying to $J/\psi$*, Phys. Lett. **B295** (1992) 396.

[39] L. Bellantoni *et al.*, Nucl. Inst. and Meth. **A310** (1991) 618.